REPORT NO.
UCB/SEMM-88/04

STRUCTURAL ENGINEERING
MECHANICS AND MATERIALS

A COMPUTATIONAL PROCEDURE FOR INTERACTION OF HIGH-SPEED VEHICLES ON FLEXIBLE STRUCTURES WITHOUT ASSUMING KNOWN VEHICLE NOMINAL MOTION

BY

LOC VU-QUOC and MATS OLSSON

(Submitted to *Computer Methods in Applied Mechanics and Engineering*.)

JANUARY 1988

DEPARTMENT OF CIVIL ENGINEERING
UNIVERSITY OF CALIFORNIA
BERKELEY, CALIFORNIA

REPORT NO.
UCB/SEMM-88/04

**STRUCTURAL ENGINEERING
MECHANICS AND MATERIALS**

A COMPUTATIONAL PROCEDURE FOR INTERACTION OF HIGH-SPEED VEHICLES ON FLEXIBLE STRUCTURES WITHOUT ASSUMING KNOWN VEHICLE NOMINAL MOTION

BY

LOC VU-QUOC and MATS OLSSON

(**Submitted to** *Computer Methods in Applied Mechanics and Engineering*.)

JANUARY 1988

**DEPARTMENT OF CIVIL ENGINEERING
UNIVERSITY OF CALIFORNIA
BERKELEY, CALIFORNIA**

A Computational Procedure for Interaction of High-Speed Vehicles on Flexible Structures without Assuming Known Vehicle Nominal Motion

By

L. Vu-Quoc† and M. Olsson‡

Abstract

An efficient and reliable computational procedure is proposed for the analysis of interaction between high-speed vehicles and flexible structures. In contrast to traditional approaches, vehicle nominal motion is considered here as unknown of the problem. The equations encountered, for vehicle motion (after elimination of algebraic constraints) and for structural motion, are in general a set of nonlinear, coupled differential equations. In spatially-discrete form, these equations do not have the form of explicit ODE's. Predictor/corrector algorithms, which combine Runge-Kutta methods and linear multistep methods with an unconditionally stable algorithm for structural dynamics, are proposed to solve the partitioned DAE's of the interaction problem. The proposed algorithms carry special features pertaining to our formulation of vehicle/structure interaction, and yield results which satisfy the essential system energy balance. The present approach effectively resolves the Timoshenko paradox in moving load problems. Several illustrative examples are presented.

Table of Contents

† Applied Mechanics Division, Stanford University, Stanford, CA 94305.

‡ Division of Structural Mechanics, Lund University, Box 118 S-221 00 Lund, Sweden. Presently visiting Structural Engineering, Mechanics, and Materials, University of California, Berkeley, CA 94720.

January 28, 1988

A Computational Procedure for Interaction of High-Speed Vehicles on Flexible Structures without Assuming Known Vehicle Nominal Motion

By

L. Vu-Quoc and M. Olsson

1. Introduction

Magnetically levitated (Maglev) vehicles will become a viable mode of high-speed transportation that bridge the gap between conventional wheel-on-rail vehicles and airplanes, for medium distances of less than a thousand kilometers. The operational speed of a Maglev is designed to reach the range of 400 to $500 km/h$ for the system to be competitive with other means of transportation in door-to-door travelling time. The noise level at this speed is comparable to that of a wheel-on-rail vehicle at $200 km/h$. Maglev systems clearly possess solid advantages with respect to the environment — energy efficient, pollution free, low noise, ecologically unobstructing due to elevation of guideways — over traditional modes of transportation. Advances in superconductor research in the future will further make these systems even more efficient and attractive. Research and development on high-speed Maglev have reached close to the stage of large scale implementation; recent reports on the status of development of Maglev systems in several countries can be found in Alscher *et al* [1983], and Eastham & Hayes [1987]. Low-speed Maglev, on the other hand, has already been put into public service, especially for short-distance transportation — less than a few kilometers (see Dalgleish & Riches [1986]).

Current state-of-the-art guideway structures for Maglev systems are designed to be stiff so that deflection falls within a very small margin of tolerance — typically about $6mm$ for a span of $25m$. As a result, the cost of guideway structure constitutes the major part (more than 70%) of the total cost of a system (Lawton [1985], Zicha [1986]). It is therefore desirable to employ more flexible guideways to reduce the total cost. This

flexibility induces, however, a complex interaction between the vehicle and its supporting guideway. In the future, progress in suspension control technology will render the use of more flexible guideways possible.

In modelling vehicle/structure interaction, one traditionally prescribes the vehicle nominal motion a-priori, thus, ignoring totally the influence of structural flexibility on the nominal motion. In Vu-Quoc & Olsson [1987,1988a], we have formulated equations of motion of a basic building-block model for analysis of complete vehicle/structure interaction, where vehicle nominal motion is part of the unknowns. This model is applicable to both wheel-on-rail vehicles and Maglev vehicles, in particular, electromagnetic systems with tight gap control (Figure 1.1). These systems have decentrally-controlled magnet units ("magnetic wheels") with constant air gap, independently of speed, in the order of 10 to $15mm$ (Eastham & Hayes [1987]). Note that the wheel model applies equally to electrodynamic Maglev vehicles which move on wheel up to a maximum lift-off speed of $80km/h$ (Alscher *et al* {1983]). Two versions of the formulation are given: a fully nonlinear version admitting finite deformation in the (beam) structure, and a mildly nonlinear version deduced from additional physically-relevant assumptions on small structural deformation. Complexity in the resulting equations arises as vehicle nominal motion is considered as unknown motion, and from the existence of convective terms, which become prominent at high speed regimes. Using an approach with prescribed nominal motion, Blejwas, Feng & Ayre [1979] have shown that it is essential to include these convective terms in the numerical formulation to obtain good corroboration of the results with experimental measures. Special numerical integration algorithms must be developed to integrate the differential equations of the mildly nonlinear version, and constitute the focus of the present paper.

In our formulation, the system of equations for vehicle/structure interaction is partitioned in two components: the vehicle motion and the structural motion. Galerkin spatial-discretization of these differential equations does *not* lead to a semi-discrete

system in the form of explicit ordinary differential equations (ODE's), but to a more general class of differential-algebraic equations (DAE's). These equations therefore do not fall into the category of partitioned ODE's, in the sense employed in Hairer [1981], often encountered in coupled-field problems such as fluid/structure or soil/structure interaction problems. Discussions on algorithms for solving coupled-field problems in engineering literature can be found for example in Park & Felippa [1983] and in Wood [1987].

Here, to solve the system of partitioned DAE's of vehicle/structure interaction, we propose predictor/corrector algorithms that share, however, a common property with algorithms for partitioned ODE's: The central idea is to employ different sub-algorithms within the same global algorithm; each of these sub-algorithms is most effective for a different component of the partitioned system.

The differential equations describing the *vehicle component* are often subjected to algebraic constraints — even for vehicles moving on a rigid structure, i.e., without the complex influence of structure flexibility. These DAE's are usually stiff for vehicle systems. Integration algorithms for DAE's have been proposed by several authors (e.g., Petzold [1982]). Führer [1986] noted, however, that when dealing with vehicle system dynamics, existing algorithms for DAE's often encounter serious problems. Consequently, transformation of DAE's into ODE's of first order form by eliminating the algebraic constraints is still de rigueur in vehicle dynamics, since this method remains the most reliable solution procedure. Führer & Wallrapp [1984] discussed methods for elimination of linear constraints, and Nikravesh [1984] for nonlinear constraints. The resulting ODE's constitute one part of the partitioned DAE's of the overall vehicle/structure system considered for the proposed algorithms in the present paper. It should be clarified that the transformed equations are considered as ODE's *only* with respect to the *vehicle* degrees of freedom. Moreover, stiff ODE's can be efficiently solved using existing specialized softwares, which are mostly based on linear multistep methods (Gupta, Sacks-Davis & Tischer [1985]).

The equations for the *structure component* are, on the other hand, solved here by efficient step-by-step implicit algorithms for second order ODE's — with respect to the structural degrees of freedom — arising in structural dynamics. These second order equations are not transformed into first order form as often done in vehicle dynamics program (see discussion in Kortüm [1986], Wallrapp [1986]). Note that the stiffness of these ODE's increases as one refines the spatial discretization of the partial differential equations (PDE's) for structural motion.‡ The implicit character of structural dynamics algorithms makes them effective tools for stiff systems in structural dynamics. Accuracy in structural motion are retained by not truncating these equations into a reduced-order model (projection onto an eigen-subspace). While the sub-algorithms for the vehicle component are highly accurate, but conditionally stable, the robustness of our proposed global algorithms is founded upon the unconditional stability of sub-algorithms for the structure component.

It should be emphasized that the equations for the two components (vehicle and structure) *together* still belong to the class of DAE's; the transformation of DAE's to ODE's mentioned earlier involves strictly the vehicle degrees of freedom. The proposed algorithms possess special features pertaining to our formulation of vehicle/structure interaction problem, and do not require evaluation of a Jacobian matrix as common in algorithms for DAE's. Good accuracy is maintained in both vehicle motion as well as in structural motion. In addition, our algorithms yield results that satisfy the essential balance of system energy. This energy balance is an important feature that not only testifies to the viability of the proposed algorithms, but also helps to effectively explain the Timoshenko paradox in moving load problems: Consider a constant vertical force traversing a simply supported beam. Basically, without a physically-complete model, one cannot explain the origin of the energy that keeps the beam in a vibratory state after the traversing of the force, since the net work done by the force is zero (cf.

‡ We refer to Dekker & Verwer [1984] for discussions on stiffness of ODE's.

Maunder [1960]).

Even though we illustrate the proposed algorithms using the basic model of vehicle/structure interaction, it should be emphasized that these algorithms are applicable to more general vehicle (with several multibody components) and structure models. Further, they can be easily incorporated in existing vehicle dynamics programs, as well as in structural dynamics programs.

Several numerical examples are presented to show that effects of complete vehicle/structure interaction can be evaluated using the present methodology. Soundness of the proposed algorithms is demonstrated in part by monitoring the offset of discrete energy balance of the system, introduced by error in the numerical results. We study the loss in velocity of a vehicle after traversing one or several spans of a continuous beam, as a result of energy transfer from the vehicle to the beam structure. Finally, we consider the braking of a vehicle, and its effects on vehicle motion and on structural response, as modeled within the present framework.

2. Equations of motion for the basic problem: Summary

To model the complete vehicle/structure interaction, we consider the basic problem of a rigid wheel, or an electromagnetic magnet with tight gap control, moving over a flexible beam. In the present work, all motions are restricted to be in a plane. We shall briefly describe the model parameters, state the basic assumptions employed in our formulation, and summarize the equations of motion obtained — the reader is referred to Vu-Quoc & Olsson [1987,1988a] for details of the derivation.

2.1. The basic model and assumptions. Figure 2.1 depicts the basic (wheel/beam) model together with its kinematic parameters. The wheel has radius R, mass M, rotatory inertia I_w. By letting $I_w \equiv 0$, one obtains a model of an electromagnetic magnet moving with constant air gap on a flexible beam as a special case of the basic model. The material (undeformed) configuration of the beam is represented by the

orthonormal basis vectors $\{\mathbf{E}_1, \mathbf{E}_2\}$, lying along the axes of a cartesian coordinate system labeled (X^1, X^2). The undeformed centroidal line of the beam, of length L, is assumed to coincide with the coordinate axis X^1. The coordinate of a material point on the centroidal line is denoted by $S \in [0,L]$. We choose $S \equiv X^1$. Let $\mathbf{Y}(t) = Y^\alpha(t)\mathbf{E}_\alpha$ denote the position of the wheel center of mass in the beam material configuration, and $t \in [0,\infty)$ the time parameter.† We call $\mathbf{Y}(t)$ the *nominal motion* of the wheel.

The basis vectors $\{\mathbf{e}_1, \mathbf{e}_2\}$ define the spatial (deformed) configuration of the beam, and are chosen such that $\mathbf{e}_i \equiv \mathbf{E}_i$, for $i = 1,2$, for convenience. Let $\mathbf{u}(S,t) = u^\alpha(S,t)\mathbf{e}_\alpha$ designate the displacement of a material point S on the centroidal line. The position of the wheel center of mass in the beam spatial configuration is denoted by $\mathbf{y}(t) = y^\alpha(t)\mathbf{e}_\alpha$. Let θ denote the revolution of the wheel. The wheel is subjected to an applied force $\mathbf{F}(t) = F^\alpha(t)\mathbf{e}_\alpha$, and a torque T about its center of mass. The contact force $\mathbf{F}_c = F_c^\alpha \mathbf{e}_\alpha$ acting on the beam is given by

$$\mathbf{F}_c = \mathbf{F} - M\ddot{\mathbf{y}} , \tag{2.1}$$

where a superposed "$\dot{}$" designates *total* time differentiation. We consider the following assumptions.

(A1) The wheel is in permanent contact with, and rolling without slipping on, the supporting beam.‡ Electromagnetic Maglev magnet ("magnetic wheel") moves with a constant air gap. The nominal motion and the actual motion of the wheel (magnet) are given by

$$\mathbf{Y}(t) = Y^1(t)\mathbf{E}_1 + \bar{R}\mathbf{E}_2 , \tag{2.2a}$$

$$y^\alpha(t) = Y^\alpha(t) + g^\alpha(\mathbf{u}(Y^1(t),t), \mathbf{u}_{,S}(Y^1(t),t)) , \text{ for } \alpha = 1,2 , \tag{2.2b}$$

with

† When the summation sign $\sum$ is absent, summation convention is implied on repeated indices, which take values in $\{1,2\}$.

‡ Note that in the case of *rigid slip*, the velocity of the contact point on the wheel is about one thousandth of the velocity of the wheel center of mass; see Kalker [1979].

$$g^1(\mathbf{u}, \mathbf{u}_{,S}) := u^1 - \bar{R}\sin\chi(\mathbf{u}_{,S}) , \quad g^2(\mathbf{u}, \mathbf{u}_{,S}) := u^2 - \bar{R}[1 - \cos\chi(\mathbf{u}_{,S})] , \tag{2.2c}$$

$$\text{and } \chi(\mathbf{u}_{,S}) := \tan^{-1}\left\{\frac{u^2{}_{,S}}{1 + u^1{}_{,S}}\right\} . \tag{2.2d}$$

where $\bar{R}$ is a constant, and the subscript ",S" denotes partial differentiation with respect to S.

(A2) The beam deforms with small strains and small rotations. The first spatial derivative of structural displacements is therefore small compared with unity: $|u^\alpha{}_{,S}| \ll 1$, for $\alpha = 1,2$. In particular, $\chi \approx u^2{}_{,S}$.

(A3) The Euler-Bernoulli hypothesis for beam deformation is assumed, leading to the strain energy expression

$$\Psi(\mathbf{u}) := \frac{1}{2}\int_{[0,\,L]} \left\{EA\,[u^1{}_{,S}]^2 + EI[u^2{}_{,SS}]^2\right\} dS , \tag{2.3}$$

where EA is the axial stiffness and EI the bending stiffness.

(A4) In the inertia operator of the equations for structural motion, only terms linear in the structural displacement u^α are retained; all nonlinear terms in u^α there are neglected.

(A5) Structural deformation has negligible effects on the revolution of the wheel such that the actual revolution is approximated by the nominal revolution:

$$\theta(Y^1,t) \approx \frac{Y^1}{R} , \quad \frac{\partial\theta(Y^1,t)}{\partial S} \approx \frac{1}{R} , \quad \dot{\theta}(Y^1,t) \approx \frac{\dot{Y}^1}{R} , \quad \ddot{\theta}(Y^1,t) \approx \frac{\ddot{Y}^1}{R} . \tag{2.4}$$

In addition, we neglect the terms with factors $\dfrac{\partial\theta}{\partial u^\beta}$ and $\dfrac{\partial\theta}{\partial u^\beta{}_{,S}}$ in the structural equations of motion.

2.2. Equations of motion. From the above assumptions, a set of mildly nonlinear differential equations describing the complete vehicle/structure interaction for the basic model is derived. These equations are naturally partitioned into two components.

The vehicle motion component. The dynamics of nominal motion Y^1 is governed by

$$c_3(Y^1,t)\ddot{Y}^1 + c_2(Y^1,t)(\dot{Y}^1)^2 + c_1(Y^1,t)\dot{Y}^1 + c_o(Y^1,t) = 0\,, \tag{2.5a}$$

where

$$c_o(Y^1,t) := -F^1[1 - \bar{R}u^2{}_{,SS}(Y^1,t)] - F^2u^2{}_{,S}(Y^1,t) - \frac{T}{R}$$

$$+ M\Big[[1 - \bar{R}u^2{}_{,SS}(Y^1,t)][u^1{}_{,tt}(Y^1,t) - \bar{R}u^2{}_{,Stt}(Y^1,t)] + u^2{}_{,S}(Y^1,t)u^2{}_{,tt}(Y^1,t)\Big], \tag{2.5b}$$

$$c_1(Y^1,t) := 2M\Big[[1 - \bar{R}u^2{}_{,SS}(Y^1,t)][u^1{}_{,St}(Y^1,t) - \bar{R}u^2{}_{,SSt}(Y^1,t)] + u^2{}_{,S}(Y^1,t)u^2{}_{,St}(Y^1,t)\Big], \tag{2.5c}$$

$$c_2(Y^1,t) := M\Big[[1 - \bar{R}u^2{}_{,SS}(Y^1,t)][u^1{}_{,SS}(Y^1,t) - \bar{R}u^2{}_{,SSS}(Y^1,t)] + u^2{}_{,S}(Y^1,t)u^2{}_{,SS}(Y^1,t)\Big], \tag{2.5d}$$

$$c_3(Y^1,t) := M[1 - \bar{R}u^2{}_{,SS}(Y^1,t)]^2 + \frac{I_w}{R^2}\,. \tag{2.5e}$$

Remark 2.1. To obtain physical insight into the above equation, consider for example the case where $F^1 = T = \bar{R} = I_w = 0$, and ignore all influence from the axial displacement u^1 of the structure. The remaining nonlinear terms in u^2 contribute to the interaction between the transverse displacement u^2 and the nominal motion Y^1, which in condensed form can be written as

$$M\ddot{Y}^1 = u^2{}_{,S}(Y^1,t)\,[\,F^2 - M\ddot{u}^2(Y^1,t)\,] \equiv u^2{}_{,S}(Y^1,t)\,F_c^2(t)\,, \tag{2.6}$$

by *total* time differentiation of u^2 together with assumption **(A2)**, and by virtue of (2.1). We have emphasized in Vu-Quoc & Olsson [1988a] the importance of the inertia force $M\ddot{u}^2$ for an adequate representation of vehicle motion at high speed. An essential feature in the present formulation is that we do not systematically neglect all nonlinear terms, but retain those which are physically relevant. □

The structural motion component. The weak form of the PDE's for structural motion in the basic model, satisfying assumptions (A1-A5), are given by (see Vu-Quoc & Olsson [1987,1988a] for more details)

$$\left[M\eta^1(Y^1,t)\left(u^1{}_{,tt}(Y^1,t)-\bar{R}u^2{}_{,Stt}(Y^1,t)\right)+\int_{[0,L]}A_\rho\eta^1(S,t)u^1{}_{,tt}(S,t)dS\right]$$

$$+\ 2M\dot{Y}^1\eta^1(Y^1,t)\left[u^1{}_{,St}(Y^1,t)-\bar{R}u^2{}_{,SSt}(Y^1,t)\right]+\left[M\eta^1(Y^1,t)\left(\ddot{Y}^1[u^1{}_{,S}(Y^1,t)-\bar{R}u^2{}_{,SS}(Y^1,t)]\right.\right.$$

$$+\ (\dot{Y}^1)^2[u^1{}_{,SS}(Y^1,t)-\bar{R}u^2{}_{,SSS}(Y^1,t)]\Big)-\bar{R}[F^1-M\ddot{Y}^1]\eta^1{}_{,S}(Y^1,t)u^2{}_{,S}(Y^1,t)$$

$$\left.+\int_{[0,L]}EA\,\eta^1{}_{,S}(S,t)u^1{}_{,S}(S,t)dS\right]=\left[\eta^1(Y^1,t)\left(F^1-M\ddot{Y}^1\right)\right], \tag{2.7a}$$

and

$$\left[-\bar{R}M\eta^2{}_{,S}(Y^1,t)\left(u^1{}_{,tt}(Y^1,t)-\bar{R}u^2{}_{,Stt}(Y^1,t)\right)+M\eta^2(Y^1,t)u^2{}_{,tt}(Y^1,t)+\int_{[0,L]}A_\rho\eta^2(S,t)u^2{}_{,tt}(S,t)dS\right]$$

$$+\ 2M\dot{Y}^1\left[-\bar{R}\,\eta^2{}_{,S}(Y^1,t)\left(u^1{}_{,St}(Y^1,t)-\bar{R}u^2{}_{,SSt}(Y^1,t)\right)+\eta^2(Y^1,t)u^2{}_{,St}(Y^1,t)\right]$$

$$+\left[M\ddot{Y}^1\left\{-\bar{R}\,\eta^2{}_{,S}(Y^1,t)\left(u^1{}_{,S}(Y^1,t)-\bar{R}u^2{}_{,SS}(Y^1,t)\right)+\eta^2(Y^1,t)u^2{}_{,S}(Y^1,t)\right\}\right.$$

$$+\ M(\dot{Y}^1)^2\left\{-\bar{R}\,\eta^2{}_{,S}(Y^1,t)\left(u^1{}_{,SS}(Y^1,t)-\bar{R}u^2{}_{,SSS}(Y^1,t)\right)+\eta^2(Y^1,t)u^2{}_{,SS}(Y^1,t)\right\}$$

$$\left.+\ \bar{R}F^2\eta^2{}_{,S}(Y^1,t)u^2{}_{,S}(Y^1,t)+\int_{[0,L]}EI\eta^2{}_{,SS}(S,t)u^2{}_{,SS}(S,t)dS\right]$$

$$=\left[-\bar{R}\,\eta^2{}_{,S}(Y^1,t)[F^1-M\ddot{Y}^1]+\eta^2(Y^1,t)F^2\right], \tag{2.7b}$$

for all admissible variations (η^1,η^2), where A_ρ denotes the mass per unit length of the beam. The terms in each of the equations in (2.7) are grouped in square brackets according to their nature (mass, velocity-convective, stiffness, and applied forces). "Velocity-convective" terms are part of the convective terms generated by taking total time derivatives — as already encountered in (2.6) — and are related to the velocity of structural deformation. A similar definition applies here to the "stiffness-convective" terms. The stiffness operators in (2.7a-b) contain, in addition to the usual terms for beam stiffness, stiffness-convective terms with $(\dot{Y}^1)^2$ and $\ddot{Y}^1$ as their factors, and terms of geometric nature with factor $\bar{R}[F^1-M\ddot{Y}^1]$ in (2.7a) and factor $\bar{R}F^2$ in (2.7b). Equations (2.5) and (2.7a-b) form a system of mildly nonlinear, coupled differential equations,

driven by initial conditions $\{Y^1(0), \dot{Y}^1(0), \mathbf{u}(S,0), \mathbf{u}_{,t}(S,0)\}$ and the forces $\{F^1, F^2, T\}$ applied on the wheel. We have now come to the central theme of the present paper, i.e., the computational procedure for solving these equations.

3. Galerkin spatial discretization: Partitioned DAE's

Spatial discretization of equations (2.5) and (2.7a-b) is discussed first. Two predictor/corrector algorithms, with a distinguished feature pertaining to our formulation, are then proposed to solve in time the resulting semi-discrete equations of motion, which are not explicit ODE's, but DAE's. We also introduce an expression for the discrete energy balance to later monitor the performance of the proposed algorithms.

For each $\alpha \in \{1,2\}$, let $\{P^\alpha_{\mathrm{I}i}(S);\ \mathrm{I} = 1,...,N;\ i = 1,...,N^\alpha\}$, be a set of independent functions in S and satisfying the essential boundary conditions for u^α. We consider the following discretization

$$\eta^\alpha(S,t) \approx \sum_{\mathrm{I}=1}^{N}\sum_{i=1}^{N^\alpha} P^\alpha_{\mathrm{I}i}(S)\eta^\alpha_{\mathrm{I}i}(t)\,, \quad u^\alpha(S,t) \approx \sum_{\mathrm{I}=1}^{N}\sum_{i=1}^{N^\alpha} P^\alpha_{\mathrm{I}i}(S)d^\alpha_{\mathrm{I}i}(t)\,. \tag{3.1}$$

The functions $P^\alpha_{\mathrm{I}i}(S)$ may be eigenfunctions in the case of a simple structure with simple boundary conditions, or finite element interpolatory functions in the case of more complex structures. Introducing the discretization (3.1) into (2.5) and (2.7) we obtain a spatially-discrete system of equations of motion. Let $n := N^1 + N^2$; then the total number of structural degrees of freedom (dof's) of the discrete system is $\nu := Nn$.† Denoting $Z := \{Y^1, \dot{Y}^1\}^{\mathrm{T}}$ and $\Delta := (\mathbf{d}, \dot{\mathbf{d}}, \ddot{\mathbf{d}})$, where $\mathbf{d}$ is the column-matrix with components $d^\alpha_{\mathrm{I}i}(t)$, the equation for the vehicle component (2.5) in our basic model could be recast into *first order* form

$$\dot{Z} = \Phi(Z, \Delta, t) := \left\{ \begin{array}{c} \dot{Y}^1 \\ \dfrac{-1}{c_3(Y^1,t)}[c_o(Y^1,t) + c_1(Y^1,t)\dot{Y}^1 + c_2(Y^1,t)(\dot{Y}^1)^2] \end{array} \right\}, \tag{3.2}$$

† For a finite element discretization, n may be thought of as the number of dof's per node, and N the number of nodal points.

where the coefficients $c_i(Y^1,t)$ are computed according to (2.5) and using the approximation (3.1). For general vehicle models, $Z = (Z^1, Z^2)$ contains all coordinates of the phase space of the vehicle motion component, with coordinates in the configuration space gathered in Z^1, and the corresponding velocities in Z^2. For the present basic model, $Z^1 \equiv Y^1$ and $Z^2 \equiv \dot{Y}^1$. It should be kept in mind, however, that the equation $\dot{Z} = \Phi(Z,\Delta,t)$ in (3.2), is intended to represent the general vehicle model — see Vu-Quoc & Olsson [1988b] for an example — in the computational procedure discussed shortly. We retain, on the other hand, the *second order* form of the equations for the structural motion component,

$$\mathbf{M}(Z)\ddot{\mathbf{d}} + \mathbf{V}(Z)\dot{\mathbf{d}} + \mathbf{S}(Z, \dot{Z})\mathbf{d} = \mathbf{R}(Z, \dot{Z}, t)\,, \tag{3.3}$$

where $\mathbf{M}(Z) \in \mathbb{R}^{\nu\times\nu}$ is the mass matrix, $\mathbf{V}(Z) \in \mathbb{R}^{\nu\times\nu}$ the velocity-convective matrix, $\mathbf{S}(Z,\dot{Z}) \in \mathbb{R}^{\nu\times\nu}$ the stiffness matrix, and $\mathbf{R}(Z,\dot{Z},t) \in \mathbb{R}^{\nu\times 1}$ the applied force matrix.

Equations (3.2) and (3.3) are nonlinear, coupled differential equations, and do not have the form of explicit ODE's. Basically, these equations form a system of DAE's of the form $G(w, \dot{w}, t) = 0$, with $w := (Z, \mathbf{d}, \dot{\mathbf{d}})$. Treatment of DAE's often requires the evaluation of the Jacobian $\partial G/\partial \dot{w}$, which is an unnecessarily complex task in the present study. In the next section, we will introduce algorithms that completely avoid evaluation of this Jacobian, and make use of the natural physical partition of the system.

Remark 3.1. In the case where finite element discretization is chosen, care should be taken in choosing interpolatory polynomials of sufficiently high order to ensure that spatial derivatives of u^α in (2.5) and (2.7) exist and are all represented. They should also be continuous across element boundaries — except when dictated by actual boundary conditions (see Examples 6.3 and 6.4). In the above equations of motion, spatial derivatives are required up to second order for u^1 and third order for u^2. Enforced continuity of these higher derivatives makes the semi-discrete system (3.2) and (3.3) well-posed, and contributes to the good behavior in numerical results. Following traditional use in finite-element analysis of (Euler-Bernoulli) beam structures, several authors (e.g., Venancio-Filho [1978], Wallrapp [1986]) employ cubic Hermitian polynomials to

interpolate the transverse displacement u^2, leading to discontinuities in $u^2{}_{,SS}$ and in $u^2{}_{,SSS}$ across element boundaries. Moreover, if linear interpolatory functions are used to approximate the axial displacement u^1, then terms in $u^1{}_{,SS}$ are artificially eliminated from the system. We note here that these discontinuities will not disappear by having more elements in the mesh, but appear on the other hand at a higher cadence. When passing over a discontinuity, often an algorithm with low order accuracy is used, unless the time step falls exactly on the discontinuity. An example of dropping in order of accuracy in the computed results due to discontinuity can be found for example in Deuflhard [1985]. □

The structure of the matrices in (3.3) could easily be written in explicit form upon rewriting (3.1) into the following form

$$\begin{Bmatrix} \eta^1(S,t) \\ \eta^2(S,t) \end{Bmatrix} \approx \sum_{\mathrm{I}=1}^{N} \mathbf{P}_{\mathrm{I}}^{o}(S)\eta_{\mathrm{I}}(t)\,, \quad \begin{Bmatrix} u^1(S,t) \\ u^2(S,t) \end{Bmatrix} \approx \sum_{\mathrm{I}=1}^{N} \mathbf{P}_{\mathrm{I}}^{o}(S)\mathbf{d}_{\mathrm{I}}(t)\,, \tag{3.4a}$$

$$\text{where} \quad \mathbf{P}_{\mathrm{I}}^{o}(S) := \begin{bmatrix} \mathbf{Q}_{\mathrm{I}}^{1}(S) & \mathbf{O}^{1\times N^2} \\ \mathbf{O}^{1\times N^1} & \mathbf{Q}_{\mathrm{I}}^{2}(S) \end{bmatrix} \in \mathbb{R}^{2\times n}\,, \tag{3.4b}$$

$$\mathbf{Q}_{\mathrm{I}}^{\alpha}(S) := \{P_{\mathrm{I}1}^{\alpha}(S), \ldots, P_{\mathrm{I}N^\alpha}^{\alpha}(S)\} \in \mathbb{R}^{1\times N^\alpha}\,, \tag{3.4c}$$

$$\eta_{\mathrm{I}}(t) := \{\eta_{\mathrm{I}1}^{1}, \ldots, \eta_{\mathrm{I}N^1}^{1}, \eta_{\mathrm{I}1}^{2}, \ldots, \eta_{\mathrm{I}N^2}^{2}\}^{\mathrm{T}} \in \mathbb{R}^{n\times 1}\,, \tag{3.4d}$$

$$\mathbf{d}_{\mathrm{I}}(t) := \{d_{\mathrm{I}1}^{1}, \ldots, d_{\mathrm{I}N^1}^{1}, d_{\mathrm{I}1}^{2}, \ldots, d_{\mathrm{I}N^2}^{2}\}^{\mathrm{T}} \in \mathbb{R}^{n\times 1}\,, \tag{3.4e}$$

with $\mathbf{O}^{i\times j}$ being the zero matrix in $\mathbb{R}^{i\times j}$. The displacement dof's of the beam structure can be ordered in $\mathbf{d}$ as follows

$$\mathbf{d}(t) = \{\mathbf{d}_1(t)^{\mathrm{T}} | \cdots | \mathbf{d}_N(t)^{\mathrm{T}}\}^{\mathrm{T}} \in \mathbb{R}^{\nu\times 1}\,. \tag{3.5}$$

Further, we define the following matrices,

$$\mathbf{P}_{\mathrm{I}}^{1}(S) := \begin{bmatrix} \mathbf{Q}_{\mathrm{I}}^{1}(S) & -\bar{R}\,\mathbf{Q}_{\mathrm{I}}^{2}{}_{,S}(S) \\ \mathbf{O}^{1\times N^1} & \mathbf{Q}_{\mathrm{I}}^{2}(S) \end{bmatrix} \in \mathbb{R}^{2\times n}\,, \tag{3.6a}$$

$$\mathbf{A}_{\mathrm{IJ}}^{1}(Z) := [\mathbf{P}_{\mathrm{I}}^{1}(Y^1)]^{\mathrm{T}}\mathbf{P}_{\mathrm{J}}^{1}{}_{,S}(Y^1) \in \mathbb{R}^{n\times n}\,, \quad \mathbf{A}_{\mathrm{IJ}}^{2}(Z) := [\mathbf{P}_{\mathrm{I}}^{1}(Y^1)]^{\mathrm{T}}\mathbf{P}_{\mathrm{J}}^{1}{}_{,SS}(Y^1) \in \mathbb{R}^{n\times n}\,, \tag{3.6b}$$

$$\mathbf{A}^3_{IJ}(Z,\dot{Z}) := \bar{R}\begin{bmatrix} \mathbf{O}^{N1\times N1} & (M\ddot{Y}^1 - F^1)[\mathbf{Q}^1_{I,S}(Y^1)]^T\mathbf{Q}^2_{J,S}(Y^1) \\ \mathbf{O}^{N2\times N1} & F^2[\mathbf{Q}^2_{I,S}(Y^1)]^T\mathbf{Q}^2_{J,S}(Y^1) \end{bmatrix} \in \mathbb{R}^{n\times n} . \tag{3.6c}$$

The mass matrix $\mathbf{M}(Z)$ can be decomposed as the sum of a constant part denoted by $\mathbf{M}^o$ and a time-varying part denoted by $\mathbf{M}^1(Z)$. Let $\mathbf{M}_{IJ}(Z) \in \mathbb{R}^{n\times n}$, for I,J $\in \{1,...,N\}$, be the submatrix of $\mathbf{M}$ that couples the dof's in $\mathbf{d}_I$ to those in $\mathbf{d}_J$; similarly for $\mathbf{M}^o_{IJ}$ and $\mathbf{M}^1_{IJ}(Z)$. Then,

$$\mathbf{M}_{IJ}(Z) = \mathbf{M}^o_{IJ} + \mathbf{M}^1_{IJ}(Z) \in \mathbb{R}^{n\times n} . \tag{3.7a}$$

We obtain from (2.7), (3.4), and (3.6a),

$$\mathbf{M}^o_{IJ} = \int_{[0,\,L]} A_\rho[\mathbf{P}^o_I(S)]^T\mathbf{P}^o_J(S)dS \in \mathbb{R}^{n\times n} , \quad \mathbf{M}^1_{IJ}(Z) = M[\mathbf{P}^1_I(Y^1)]^T\mathbf{P}^1_J(Y^1) \in \mathbb{R}^{n\times n} . \tag{3.7b}$$

It should be noted here that the mass matrix is symmetric, i.e., $\mathbf{M}_{IJ} = \mathbf{M}_{JI}$. However, such is not the case for the velocity-convective matrix $\mathbf{V}$ and the stiffness matrix $\mathbf{S}$ as will be seen shortly. From (2.7) and using the definitions in (3.6), an expression for $\mathbf{V}(Z)$ can be readily obtained as

$$\mathbf{V}_{IJ}(Z) = 2M\dot{Y}^1\mathbf{A}^1_{IJ}(Z) \in \mathbb{R}^{n\times n} . \tag{3.8}$$

Analogous to the mass matrix $\mathbf{M}(Z)$, the stiffness matrix $\mathbf{S}(Z,\dot{Z})$ is split up into a constant part $\mathbf{S}^o$ and a time-varying part $\mathbf{S}^1(Z,\dot{Z})$ whose expressions are given by

$$\mathbf{S}_{IJ}(Z,\dot{Z}) = \mathbf{S}^o_{IJ} + \mathbf{S}^1_{IJ}(Z,\dot{Z}) \in \mathbb{R}^{n\times n} , \tag{3.9a}$$

$$\mathbf{S}^o_{IJ} := \int_{[0,\,L]} \begin{bmatrix} EA\,[\mathbf{Q}^1_{I,S}(S)]^T\mathbf{Q}^1_{J,S}(S) & \mathbf{O}^{N1\times N2} \\ \mathbf{O}^{N2\times N1} & EI[\mathbf{Q}^2_{I,SS}(S)]^T\mathbf{Q}^2_{J,SS}(S) \end{bmatrix} dS \in \mathbb{R}^{n\times n} , \tag{3.9b}$$

$$\mathbf{S}^1_{IJ}(Z,\dot{Z}) := M\ddot{Y}^1\mathbf{A}^1_{IJ}(Z) + M(\dot{Y}^1)^2\mathbf{A}^2_{IJ}(Z) + \mathbf{A}^3_{IJ}(Z,\dot{Z}) \in \mathbb{R}^{n\times n} . \tag{3.9c}$$

The first two terms in (3.9c) are convective terms, whereas the last term, $\mathbf{A}^3_{IJ}(Z,\dot{Z})$, expresses the geometric effect induced by the constraints (2.2). Finally, the applied force column-matrix corresponding to the degrees of freedom in $\mathbf{d}_I$ is

$$\mathbf{R}_I(Z,\dot{Z},t) = [\mathbf{P}^1_I(Y^1)]^T\begin{Bmatrix} F^1 - M\ddot{Y}^1 \\ F^2 \end{Bmatrix} \in \mathbb{R}^{n\times 1} . \tag{3.10}$$

Remark 3.2. The global matrices acquire a particular structure when Galerkin finite-element discretization is used: The time-varying matrices $\mathbf{M}^1(Z)$, $\mathbf{V}(Z)$, and $\mathbf{S}^1(Z,\dot{Z})$ contain zero coefficients except in a small submatrix located on their diagonal. For a discretization of the type (3.4), this submatrix is of dimension $2n \times 2n$ for an element with two nodal points. Note that we are concerned here with the basic model with one wheel (magnet); in a general vehicle model, there is a submatrix of the above type for each wheel (magnet). As the wheel moves (say, in the direction of increasing node numbers), the time-varying submatrices charge down along the diagonal of the global matrices.§ The reason for this particular structure of the time-varying matrices is the local character of finite element basis functions (functions with compact support). Similar observation could be made regarding the applied force $\mathbf{R}(Z,\dot{Z},t)$. However, if the functions $P_{\mathrm{li}}^{\alpha}(S)$, are eigenfunctions of a vibrating beam, then all of the above matrices are full — but possibly of smaller order. □

4. Predictor/corrector temporal discretization

We are now ready to introduce discretization in time to solve the partitioned DAE's with vehicle component (3.2) and structure component (3.3). In the general setting where a complex vehicle model (multibody system) is involved, the number of equations in $\dot{Z} = \Phi(Z,\Delta,t)$ for the vehicle component, i.e., the dimension of the phase space of for vehicle motion, could be of the same order as the number of equations for the structure component. It is noted that our numerical treatment in this section, even though applied to the basic model in examples of Section 6, extends to the above general setting.

§ In a particular case of the present formulation, where only a point mass is considered ($I_w = 0$) with prescribed nominal motion, and where $\mathbf{A}_{\mathrm{lJ}}^{3}(Z) \equiv 0$, the element matrices corresponding to the loaded element are referred to as "structure/vehicle element" in Olsson [1985,1986].

In many simulation programs for vehicle dynamics, a reduced-order model for the structure is obtained by projecting (3.3) onto a subspace of eigenvectors (see, e.g., Wallrapp [1986] in relation to the program MEDYNA),† and implies a frequency cut-off in the structural response. This reduced-order model is then transformed into first order ODE's;‡ the cost of transforming a large system in (3.3) into first order form and of subsequent numerical solution being prohibitively expensive. Choice of the subspace of eigenvectors must be made carefully to represent all relevant effects in the motion, which are often difficult to guess in advance. The reason of this caution rests on the fact that the choice of an eigen-subspace that contains the maximum information on the motion depends intimately on the applied forces, i.e., a systematic selection of low frequency modes may lead to a misrepresentation of the motion. Further, recall that the projected matrices lose their bandedness, and are thus fully populated. In this paper, we propose two predictor/corrector methods for integrating (3.2) and (3.3) which retain the efficiency of structural dynamics algorithms for solving the unreduced system (3.3).

In what follows, the subscript $k+\varsigma_i$ will be used to designate the discrete approximate of a quantity at time $t_{k+\varsigma_i} \equiv t_k + \varsigma_i h$, where $\varsigma_i \in [0, 1]$, and h denotes the current time step size. Thus, for a function $f(t)$, we write $f_{k+\varsigma_i} \approx f(t_{k+\varsigma_i})$. The approximate to the structural displacement defined in (3.5) is written as $\mathbf{d}_{k+\varsigma_i} \approx \mathbf{d}(t_{k+\varsigma_i})$. Similarly, structural velocity and acceleration at time $t_{k+\varsigma_i}$ are denoted by $\mathbf{v}_{k+\varsigma_i} \approx \dot{\mathbf{d}}(t_{k+\varsigma_i})$ and $\mathbf{a}_{k+\varsigma_i} \approx \ddot{\mathbf{d}}(t_{k+\varsigma_i})$, respectively. Hence, $\Delta_{k+\varsigma_i} = (\mathbf{d}_{k+\varsigma_i}, \mathbf{v}_{k+\varsigma_i}, \mathbf{a}_{k+\varsigma_i})$. Further, we define the matrix $\mathbf{d}^\alpha$ whose coefficients are all the dof's corresponding to u^α

$$\mathbf{d}^\alpha := \{d^\alpha_{11}, \ldots, d^\alpha_{1N^\alpha} \mid \cdots \mid d^\alpha_{N1}, \ldots, d^\alpha_{NN^\alpha}\}^{\mathrm{T}} \in \mathbb{R}^{(NN^\alpha)\times 1}\,, \tag{4.1a}$$

and thus

$$\mathbf{v}^\alpha_{k+\varsigma_i} \approx \dot{\mathbf{d}}^\alpha(t_{k+\varsigma_i})\,, \quad \mathbf{a}^\alpha_{k+\varsigma_i} \approx \ddot{\mathbf{d}}^\alpha(t_{k+\varsigma_i})\,. \tag{4.1b}$$

† These eigenvectors correspond to the eigenvalue problem $\mathbf{S}^o\mathbf{x} = \lambda\mathbf{M}^o\mathbf{x}$.

‡ Vehicle nominal motion is prescribed a-priori in this work.

The notation $\left(v_{Ii}^{\alpha}\right)_{k+\varsigma_i} \approx \dot{d}_{Ii}^{\alpha}(t_{k+\varsigma_i})$ and $\left(a_{Ii}^{\alpha}\right)_{k+\varsigma_i} \approx \ddot{d}_{Ii}^{\alpha}(t_{k+\varsigma_i})$ will also be used. In addition, we introduce the following expressions

$$\mathbf{K}(Z_{k+\varsigma_i}) := \left[\mathbf{M}(Z_{k+\varsigma_i}) + \varsigma_i h(\tfrac{3}{2}-\gamma)\mathbf{V}(Z_{k+\varsigma_i}) + \frac{\varsigma_i^2 h^2}{4\gamma^2}\,\mathbf{S}(Z_{k+\varsigma_i})\right] \in \mathbb{R}^{\nu\times\nu}, \tag{4.2a}$$

$$\begin{aligned}\mathbf{f}(Z_{k+\varsigma_i}, t_{k+\varsigma_i}) := {}& \mathbf{R}(Z_{k+\varsigma_i}, t_{k+\varsigma_i}) - \mathbf{V}(Z_{k+\varsigma_i})[\mathbf{v}_k + \varsigma_i h(2\gamma - \tfrac{3}{2})\mathbf{a}_k] \\ & - \mathbf{S}(Z_{k+\varsigma_i})\left[\mathbf{d}_k + \varsigma_i h\gamma\mathbf{v}_k + \frac{\varsigma_i^2 h^2}{2}\left(1 - \frac{1}{2\gamma^2}\right)\mathbf{a}_k\right] \in \mathbb{R}^{\nu\times 1},\end{aligned} \tag{4.2b}$$

$$\mathbf{v}_{k+\varsigma_i} = \mathbf{v}_k + \varsigma_i h\left[(\gamma - \tfrac{1}{2})\mathbf{a}_k + (\tfrac{3}{2}-\gamma)\mathbf{a}_{k+\varsigma_i}\right] \in \mathbb{R}^{\nu\times 1}, \tag{4.3a}$$

$$\mathbf{d}_{k+\varsigma_i} = \mathbf{d}_k + \varsigma_i h\mathbf{v}_k + \frac{\varsigma_i^2 h^2}{2}\left[\left(1 - \frac{1}{2\gamma^2}\right)\mathbf{a}_k + \frac{1}{2\gamma^2}\,\mathbf{a}_{k+\varsigma_i}\right] \in \mathbb{R}^{\nu\times 1}, \tag{4.3b}$$

where γ is an algorithm constant, and where the shorthand notations $\mathbf{S}(Z) \equiv \mathbf{S}(Z,\dot{Z})$ and $\mathbf{R}(Z,t) \equiv \mathbf{R}(Z,\dot{Z},t)$ have been used to alleviate notation.

4.1. Single-step method. The following algorithm is a single-step predictor/corrector that combines explicit methods of the Runge-Kutta family with an efficient algorithm in structural dynamics for solving (3.2) and (3.3).

Algorithm 1: (single-step predictor/corrector)

Data:
- Algo. const.: γ, p, $\{\varsigma_i;\ i=1,\ldots,p\}$, $\{a_{ij};\ i=2,\ldots,p,\ j=1,\ldots,(i-1)\}$, $\{b_i;\ i=1,\ldots,p\}$,
- Current time step size h,
- Solution at time t_k: Z_k, $\mathbf{d}_k$, $\mathbf{v}_k$, $\mathbf{a}_k$.

Predictor:

1) $D_1 = h\Phi(Z_k, \Delta_k, t_k)$.

For each $(i \in \{2,\ldots,p\})$, **do** {

2) $\hat{Z}_{k+\varsigma_i} = Z_k + \sum_{j=1}^{i-1} a_{ij} D_j$.

3) Solve for $\hat{\mathbf{a}}_{k+\varsigma_i}$ such that $\mathbf{K}(\hat{Z}_{k+\varsigma_i})\,\hat{\mathbf{a}}_{k+\varsigma_i} = \mathbf{f}(\hat{Z}_{k+\varsigma_i}, t_{k+\varsigma_i})$, where $\mathbf{K}$ and $\mathbf{f}$ are computed as in (4.2).

4) *Displacement*: Compute $\hat{\mathbf{d}}_{k+\varsigma_i}$ using $\hat{\mathbf{a}}_{k+\varsigma_i}$ as in (4.3b).

5) *Axial velocity*: Set $\left(\hat{v}_{Ij}^{1}\right)_{k+\varsigma_i} \equiv \left(v_{Ij}^{1}\right)_k$ if $Z^1 \cap \operatorname{supp} P_{Ij}^{1} \neq \varnothing$

for I = 1,...,N and j = 1,...,N^1.†

Transverse velocity: Compute $\hat{\mathbf{v}}^2_{k+\varsigma_i}$ using $\hat{\mathbf{a}}^2_{k+\varsigma_i}$ as in (4.3a).

6) *Axial acceleration*: Set $\left(\hat{a}^1_{Ij}\right)_{k+\varsigma_i} \equiv 0$ if $Z^1 \cap \text{supp}\, P^1_{Ij} \neq \varnothing$

for I = 1,...,N and j = 1,...,N^1.

7) $D_i = h\Phi(\hat{Z}_{k+\varsigma_i}, \hat{\Delta}_{k+\varsigma_i}, t_{k+\varsigma_i})$.

}

Corrector:

8) $Z_{k+1} = Z_k + \sum_{i=1}^{p} b_i D_i$.

9) Solve for $\mathbf{a}_{k+1}$ such that $\mathbf{K}(Z_{k+1})\, \mathbf{a}_{k+1} = \mathbf{f}(Z_{k+1}, t_{k+1})$, where $\mathbf{K}$ and $\mathbf{f}$ are computed as in (4.2).

10) Compute $\mathbf{v}_{k+1}$ and $\mathbf{d}_{k+1}$ using $\mathbf{a}_{k+1}$ as in (4.3).

□

Remark 4.1. Assuming that the structural displacement $\mathbf{d}(t)$ is known exactly for all $t \in [0,+\infty)$ then with $\mathbf{d}_k \equiv \mathbf{d}(t_k)$, $\forall\ k$, Steps 1,2,7 and 8 in Algorithm **1** constitute the explicit p-stage Runge-Kutta method, with coefficients ς_i, a_{ij} and b_i, and solving for $Z(t)$. For instance, the 4-stage classical Runge-Kutta method (4th-order accurate) has coefficients $\{\varsigma_i\} = \{0, \frac{1}{2}, \frac{1}{2}, 1\}$, $a_{ij} = 0$ except $\{a_{21}, a_{32}, a_{43}\} = \{\frac{1}{2}, \frac{1}{2}, 1\}$, and $\{b_i\} = \{\frac{1}{6}, \frac{1}{3}, \frac{1}{3}, \frac{1}{6}\}$.‡ Higher order Runge-Kutta methods such as those proposed by Dormand & Prince [1978] could also be used.§ Consider the partition $\Phi \equiv (\Phi^1, \Phi^2)$ and $D_i \equiv (D_i^1, D_i^2)$ in the same manner as in $Z \equiv (Z^1, Z^2)$. Then when $\Phi^1 \equiv Z^2$, as in the present basic model, one can dispense with the coefficients D_i^1, and rearrange the computation more efficiently as follows. Let

$$b^* := \sum_{i=1}^{p} b_i\ , \quad \bar{b}_j := \sum_{i=j+1}^{p} b_i\, a_{ij}\ . \tag{4.4a}$$

In Step 1, compute $D_1^2 \equiv h\Phi^2(Z_k, \Delta_k, t_k)$.

In Step 7, for i = 2,...,p, compute $D_i^2 = h\Phi^2(\hat{Z}_{k+\varsigma_i}, \hat{\Delta}_{k+\varsigma_i}, t_{k+\varsigma_i})$.

† The support of a function f is denoted by supp$f$.

‡ A *convention* often valid for almost all Runge-Kutta schemes is: $\varsigma_i = \sum_{j=1}^{p} a_{ij}$ (see Dekker & Verwer [1984]).

§ See for example Butcher [1987] for detailed discussions on explicit Runge-Kutta methods.

In Step 8, $Z_{k+1} = (Z^1_{k+1},\, Z^2_{k+1})$ is then computed by

$$Z^1_{k+1} = Z^1_k + hb^* Z^2_k + h\sum_{i=1}^{p-1} \bar{b}_i D_i^2\,, \quad Z^2_{k+1} = Z^2_k + \sum_{i=1}^{p} b_i D_i^2\,. \tag{4.4b}$$

This procedure is equivalent to the Nyström method in terms of efficiency. Recall that the Nyström method (see, e.g., Fine [1987]) deals directly with the second order equations $\ddot{Z}^1 = \Phi^2(Z^1,\dot{Z}^1,\Delta,t)$, and is most efficient only when Φ^2 is not function of $\dot{Z}^1$, which is not true in our case. □

Remark 4.2. If the nominal motion $Y^1(t)$ (or $Z(t)$) is known a-priori, then with $Z_{k+1} \equiv Z(t_{k+1})$, $\forall\ k$, Steps 9 and 10 in Algorithm **1** express balance of momentum at time t_{k+1}, and correspond to the implicit "θ_1-method" proposed by Hoff [1986]. We note that to derive (4.2a-b) from the balance of momentum (3.3) at time $t_{k+\varsigma_i}$, the following relations are used

$$\mathbf{v}_{k+\varsigma_i} = \mathbf{v}_k + \varsigma_i h\left[(2\gamma - \tfrac{3}{2})\mathbf{a}_k + (\tfrac{3}{2} - \gamma)\mathbf{a}_{k+\varsigma_i}\right] \in \mathbb{R}^{\nu\times 1}\,, \tag{4.5a}$$

$$\mathbf{d}_{k+\varsigma_i} = \mathbf{d}_k + \varsigma_i h\gamma\mathbf{v}_k + \frac{\varsigma_i^2 h^2}{2}\left[\left(1 - \frac{1}{2\gamma^2}\right)\mathbf{a}_k + \frac{1}{2\gamma^2}\,\mathbf{a}_{k+\varsigma_i}\right] \in \mathbb{R}^{\nu\times 1}\,. \tag{4.5b}$$

These relations are slightly different from (4.3a-b), and effectively introduce numerical dissipation in the high frequencies (for $\gamma < 1$). This algorithm is unconditionally stable for $\gamma \in [0.5,\, 1]$, and is (locally) second order accurate. However, in order to have no overshooting, small algorithmic damping, and small relative period error, it is recommended to use $\gamma \in [0.95,\, 1]$ (Hoff & Pahl [1987]). For $\gamma = 1$, the method reduces to the trapezoidal rule with well understood properties (see, e.g., Hughes [1983]). We note that either displacement or velocity, instead of acceleration as presented in Steps 3 and 9, could be equivalently chosen as primary unknown. The "θ_1-method" is close to the trapezoidal rule in the low frequency range, and offers numerical dissipation in the high frequency range. The main motivation in using this type of method to obtain the mentioned "low-pass filtering" effect is because spatial discretization of related PDE's often yields worse accuracy for high frequency response than for low frequency response.

Recall on the other hand that the trapezoidal rule is free of numerical dissipation in the whole frequency range, and is thus able to reflect with fidelity properties of the spatial discretization. □

The "θ_1-method" (implicit, unconditionally stable) is employed here to predict structural response for the intermediate steps of the Runge-Kutta scheme (explicit, conditionally stable) with a special treatment for axial motion: In the computation of D_i, for $i = 2,...,p$, if $Z^1 \cap \text{supp}\, P^1_{Ij} \neq \emptyset$(i.e., the support of P^1_{Ij} contains at least one wheel or magnet) then the axial velocity $\hat{v}^1_{Ij}$ at time $t_{k+\varsigma_i}$ is reset to its value at time t_k (see Step 5), while the axial acceleration $\hat{a}^1_{Ij}$ at time $t_{k+\varsigma_i}$ is reset to zero (see Step 6), and this for $I = 1,...,N$ and $j = 1,...,N^1$. Recall that in a general vehicle model, Z^1 is the set of nominal positions of the vehicle wheels or magnets. Instead of Steps 5 and 6, we could have retained the axial acceleration as computed in Step 3, and evaluate the axial velocity according to (4.3a). The above treatment is, however, found to effectively maintain stability of the numerical algorithm by preventing high oscillations with unbounded growth of energy, as will be demonstrated in numerical examples below. Explanation of the mechanism triggering this growth in energy is deferred until later in the examples section.

Remark 4.3. In Steps 4 and 5, in the computation of the displacement $\hat{\mathbf{d}}_{k+\varsigma_i}$ and transverse velocity $\hat{\mathbf{v}}^2_{k+\varsigma_i}$, we only need to compute those coefficients that correspond to the functions P^α_{Ii} whose supports contain at least one wheel or magnet in a general vehicle model, i.e., $Z^1 \cap \text{supp}\, P^\alpha_{Ii} \neq \emptyset$. □

We mention in passing that for systems with constant coefficients, the "θ_1-method" shares similar properties with the "α-method" proposed by Hilber, Hughes & Taylor [1977]. The former possesses some advantages over the latter, but more importantly, lends itself nicely to nonlinear systems with time-varying coefficients. Other type of single-step structural dynamics algorithms, such as the "beta-m" method by Katona & Zienkiewicz [1985], could also be employed. However, explicit integration methods, even

with high order of accuracy, are not recommended for this problem because of their severe restriction on the time step size (conditional stability). An unconditionally stable "explicit" algorithm was proposed by Trujillo [1972],† but suffers poor accuracy (Belytschko [1983]). Further, a foremost advantage of explicit methods over implicit methods rests on the constancy of the mass matrix (or better yet, a diagonal mass matrix). This advantage is quickly nullified if the mass matrix is non-diagonal, and has time-dependent coefficients such as in the present study. A recent state-of-the-art review by Wood [1987] provides an extensive survey into numerical integrators employed in structural dynamics. A word of caution is here warranted: Since most of these algorithms are analyzed for a scalar differential equation (except the algorithm by Gellert [1978]) with constant coefficients, their properties should not be freely extended to systems with time-varying coefficients and with non-diagonalizable "damping" matrix (here, the velocity-convective term‡) as that encountered in the present study. Gear [1978] had in fact warned about the danger of employing such algorithms for non-diagonalizable systems. In our problem, we found that the trapezoidal rule was definitely adequate.

4.2. Linear multistep method. In Algorithm **1**, each iteration i in the predictor stage requires solving a system of linear equations to predict the structural motion. This process, often referred to as function evaluation, is particularly an expensive step in our problem. In addition, as mentioned in the introduction, differential equations for the vehicle component are often stiff. Implicit Runge-Kutta methods can offer A-stability, which is desirable to treat stiff ODE's, together with high accuracy. However, solution of the resulting nonlinear algebraic equations often make these methods prohibitively expensive (Gupta, Sacks-Davis & Tischer [1985]). On the other hand, linear multistep methods require less function evaluations than single-step (explicit) Runge-Kutta methods, and therefore will prove to be advantageous in decreasing computational effort

† This method is based on application of operator splitting to the trapezoidal rule, which is an unconditionally stable implicit method, to avoid solving a system of linear equations.
§ This matrix does *not* represent any real damping effects in the system.

in the present study.‡ Further, these methods can also handle effectively stiff ODE's. We consider therefore in Algorithm **2** a combination of linear multistep methods and the "θ_1-method." Let

$$\Phi_k^{[i]} := \Phi^{[i]}(Z_k, \Delta_k, t_k), \quad \text{where} \quad \Phi^{[i]} := \frac{d^{i+1}Z}{dt^{i+1}}, \quad \text{and} \quad \Phi^{[0]} \equiv \Phi . \tag{4.6}$$

Algorithm 2: (linear multistep predictor/corrector)

Data:
- Algo. const.: γ, q, m, $\{\alpha_i, \beta_i;\ i=1,...,q\}$, $\{\lambda_i, \mu_i;\ i=0,...,(q-1)\}$,
- Current time step size h,
- Solution at time t_k: $\{Z_k, \Phi_k^{[0]}, \ldots, \Phi_k^{[q]}\}$, $\mathbf{d}_k$, $\mathbf{v}_k$, $\mathbf{a}_k$.

Predictor (P):

1) Compute $\{\Phi_{k-1}, \ldots, \Phi_{k-q+1}\}$ from $\{\Phi_k^{[0]}, \ldots, \Phi_k^{[q]}\}$.
2) $Z_{k+1}^{(0)} = \sum_{j=1}^{q} [\alpha_j Z_{k-j+1} + h\beta_j \Phi_{k-j+1}]$.
3) Solve for $\mathbf{a}_{k+1}^{(0)}$ such that $\mathbf{K}(Z_{k+1}^{(0)})\, \mathbf{a}_{k+1}^{(0)} = \mathbf{f}(Z_{k+1}^{(0)}, t_{k+1})$, where $\mathbf{K}$ and $\mathbf{f}$ are computed as in (4.2).
4) *Displacement*: Compute $\mathbf{d}_{k+1}^{(0)}$ using $\mathbf{a}_{k+1}^{(0)}$ as in (4.3b).
5) *Axial velocity*: Set $\left(v_{Ij}^1\right)_{k+1}^{(0)} \equiv \left(v_{Ij}^1\right)_k$ if $Z^1 \cap \operatorname{supp} P_{Ij}^1 \neq \varnothing$, for I = 1,...,$N$ and j = 1,...,N^1.
   Transverse velocity: Compute $\left(\mathbf{v}^2\right)_{k+1}^{(0)}$ using $\left(\mathbf{a}^2\right)_{k+1}^{(0)}$ as in (4.3a).
6) *Axial acceleration*: Set $\left(a_{Ij}^1\right)_{k+1}^{(0)} \equiv 0$ if $Z^1 \cap \operatorname{supp} P_{Ij}^1 \neq \varnothing$ for I = 1,...,N and j = 1,...,N^1.

Corrector $(\mathrm{EC})^m$:

For each ($i \in \{1,...,m\}$), **do** {

7) Evaluate $\Phi_{k+1} = \Phi(Z_{k+1}^{(i-1)}, \Delta_{k+1}^{(i-1)}, t_{k+1})$.
8) $Z_{k+1}^{(i)} = \sum_{j=0}^{q-1} [\lambda_j Z_{k-j} + h\mu_j \Phi_{k-j+1}]$.
9) Solve for $\mathbf{a}_{k+1}^{(i)}$ such that $\mathbf{K}(Z_{k+1}^{(i)})\, \mathbf{a}_{k+1}^{(i)} = \mathbf{f}(Z_{k+1}^{(i)}, t_{k+1})$, where $\mathbf{K}$ and $\mathbf{f}$ are computed as in (4.2).
10) Compute $\mathbf{v}_{k+1}^{(i)}$ and $\mathbf{d}_{k+1}^{(i)}$ using $\mathbf{a}_{k+1}^{(i)}$ as in (4.3).

}

11) *Evaluation* (E): $\Phi_{k+1} = \Phi(Z_{k+1}^{(m)}, \Delta_{k+1}^{(m)}, t_{k+1})$.

□

‡ In general, when solving ODE's, one should also account for the overhead cost. Then linear multistep methods do not necessarily come out as winners over Runge-Kutta methods (Gupta [1980]).

Remark 4.4. In the above, Step 2 contains the q-step Adams-Bashford method and Crane-Klopfenstein method, whereas Step 5 may be specialized to the $(q-1)$-step Adams-Moulton method, with m being the number of simple iterations in the corrector stage (see, e.g., Lambert [1973]). For $q = 4$, the 4-step Adams-Bashford method has coefficients

$$\alpha_1 = 1\,, \quad \alpha_2 = \alpha_3 = \alpha_4 = 0\,, \quad \text{and} \quad \{24\beta_i\} = \{55, -59, 37, -9\}\,,$$

while the Crane-Klopfenstein method has coefficients

$\alpha_1 = \quad 1.547652$	$\beta_1 = \quad 2.002247$
$\alpha_2 = -1.867503$	$\beta_2 = -2.031690$
$\alpha_3 = \quad 2.017204$	$\beta_3 = \quad 1.818609$
$\alpha_4 = -0.697353$	$\beta_4 = -0.714320$

and the 3-step Adams-Moulton method has coefficients

$$\lambda_0 = 1\,, \quad \lambda_1 = \lambda_2 = \lambda_3 = 0\,, \quad \text{and} \quad \{24\mu_i\} = \{9, 19, -5, 1\}\,. \quad \square$$

Remark 4.5. In step 1, with the step size h given, the value of $\{\Phi_{k-1}, \ldots, \Phi_{k-q+1}\}$ from $\{\Phi_k^{[0]}, \ldots, \Phi_k^{[q]}\}$ (and vice versa) is easily obtained by interpolation of a polynomial of degree q (see, e.g., Gear [1971, p.149]). This procedure (due to Nordsieck) allows a convenient change of time step size. $\square$

Algorithm **2** is a general predictor/corrector in $P(EC)^m E$ mode. For $m = 1$ and $q = 4$, the Crane-Klopfenstein predictor combined with the 3-step Adams-Moulton corrector is of 4th-order, and has a region of absolute stability comparable to that of the classical (4th-order) Runge-Kutta method. This region of absolute stability is more than twice larger than that of the Adams-Bashford-Moulton method in both $P(EC)^2$ mode and in *PECE* mode (Lambert [1973, p.148]). Even though the two Algorithms **1** and **2** (when using the above coefficients) have similar properties regarding accuracy and stability, the computational effort in Algorithm **2** with *PECE* mode is twice less: It requires

only two solutions for structural motion, instead of four as in Algorithm **1**. Therefore, Algorithm **2** is definitely more efficient than Algorithm **1**, except that it is not self-starting. We will use the latter to create starting points for the former. Note that Remark 4.3 also applies for Steps 4 and 5 of Algorithm **2**.

Even though more efficient starters based on methods proposed by Gear [1980] could be developed, but considering that the overall saving is not significant, in the present work, all results are reported with Algorithm **1** as starter for Algorithm **2**. An alternative to this starting procedure would be to use low-order methods with small step size at the beginning. The robustness of the proposed predictor/corrector algorithms rests in part on the choice of unconditionally stable sub-algorithms for the structural motion component; recall that sub-algorithms for the vehicle motion component are only conditionally stable. Methods other than linear multistep ones, such as extrapolation methods, could be explored as alternatives (Gupta, Sacks-Davis & Tischer [1985]). Deuflhard [1985] provides an extensive review of extrapolation methods. Finally, we note that the proposed algorithms are extendible to the case with fully nonlinear beam theory (see Vu-Quoc [1986] and Vu-Quoc & Simo [1988] for a related algorithm to solve an ODE/PDE system arising in satellite dynamics).

5. Discrete energy balance

The balance of system energy at time t can be written as follows

$$\mathcal{K}_t + \Psi_t - \int_0^t [\, F^\alpha(\tau)\dot{y}^\alpha(\tau) + T(\tau)\dot{\theta}(\tau)\,]\, d\tau = \mathcal{K}_o + \Psi_o\,, \tag{5.1}$$

where $\mathcal{K}_t$ and Ψ_t are the current kinetic energy and potential energy, the integral term is the work done by external forces, $\mathcal{K}_o$ the initial kinetic energy, and Ψ_o the initial potential energy. For small structural deformations, we consider the following approximation to the kinetic energy and potential energy

$$\mathcal{K}_t \approx \frac{1}{2} M\left\{[\dot{Y}^1 + \dot{u}^1(Y^1,t) - \bar{R}\dot{u}^2{}_{,S}(Y^1,t)]^2 + [\dot{u}^2(Y^1,t)]^2\right\} + \frac{1}{2} I_w \left(\frac{\dot{Y}^1}{R}\right)^2 + \frac{1}{2}\,\dot{\mathbf{d}}^{\mathrm{T}}\mathbf{M}^e\dot{\mathbf{d}}\,, \tag{5.2a}$$

$$\Psi_t \approx \frac{1}{2}\,\mathbf{d}^{\mathrm{T}}\,\mathbf{S}^{o}\,\mathbf{d}\,, \tag{5.2b}$$

where $\overset{\bullet}{u}{}^{\alpha}$ is to be interpreted in terms of *total* time derivative. It is important to note that, despite the approximation in the velocity already employed in (5.2a), to obtain (2.5) and (2.7), further reductions should be made to the Euler-Lagrange equations derived from using this approximated kinetic energy. Nevertheless, for small deformations, this is a good approximation for an energy balance check in the numerical results. The use of (5.1) and (5.2) together provide a useful guideline in the design of numerical integration methods. We will show by numerical examples that the proposed algorithms maintain well energy balance to within very small error tolerance. Recall that in linear structural dynamics, the trapezoidal rule preserves exactly system energy (e.g., Hughes [1983]). In addition to providing an indication to the soundness of integration algorithms, energy balance is used to explain the Timoshenko paradox mentioned in the introduction.

6. Numerical examples

In this section, numerical results for our basic model of vehicle/structure interaction are presented for a wide range of vehicle speeds. These examples demonstrate the reliability and efficiency of the proposed integration algorithms, as well as the adequacy of the present formulation for vehicles moving at high speed on flexible structures. Emphasis is focused on results which are not achievable using formulations based on the traditional assumption of known vehicle nominal motion.

Finite element basis functions are used here in the discretization (3.4) such that for a partition $0 \equiv S_1 < \ldots < S_N \equiv L$, the dof's associated with node $\mathrm{I} \in \{1,\ldots,N\}$ are the displacement components and their spatial derivatives (see (3.4e)):

$$d^{\alpha}_{\mathrm{Ii}} \approx \frac{\partial^{i-1} u^{\alpha}(S_{\mathrm{I}},t)}{\partial S^{i-1}}\,. \tag{6.1}$$

For complete continuity of the spatial derivatives appearing in (2.5) and (2.7), one

should use (at least) $N^1 = 3$ for the axial dof's, and $N^2 = 4$ for the transverse dof's. There are thus seven dof's at each nodal point. It is easy to construct the basis functions P_{li}^{α} corresponding to these dof's in terms of polynomials: For the axial displacement, P_{li}^1 are 5th-order polynomials, while for the transverse displacement P_{li}^2 are 7th-order polynomials.

The proposed computational procedure for analyzing vehicle/structure interaction has been implemented in the research version of FEAP, the Finite Element Analysis Program developed by R.L. Taylor — see Zienkiewicz [1977, Chap. 24] for a description of a simple version, and compiled under the Berkeley Unix 4.3 BSD operating system. The beam element used in our work is implemented to allow the flexibility to choose different number of nodal dof's, i.e., different values of N^1 and N^2.

All numerical results reported herein are obtained with the following algorithm constants. In Algorithm **1**, we use the constants for the classical Runge-Kutta method (Remark 4.1), and in Algorithm **2** the constants for the Crane-Klopfenstein and the Adams-Moulton methods (Remark 4.4). The *PECE* mode is chosen for Algorithm **2** ($m = 1$), with starting points generated by using Algorithm **1**. Integration of structural motion is performed with $\gamma = 1$, i.e., the trapezoidal rule. In all examples, the time step size is kept constant throughout the calculation. Also, all beam structures and their spatial discretizations are uniform. Effects of complete vehicle/structure interaction will be studied in the following examples for a simple-span and a six-span beam structure depicted in Figure 6.0.

Example 6.1. Vehicle traversing a simple-span guideway. Consider a wheel of mass $M = 3000kg$, rotatory inertia $I_w = 135kgm^2$, radius $R = 0.3m$, rolling over a simply supported beam. The distance from the beam centroidal line to the wheel center of mass is $\bar{R} = 0.9m$. The beam has a length $L = 24m$, mass per unit length $A_\rho = 1250kg/m$, axial stiffness $EA = 5\times 10^9 N$, and bending stiffness $EI = 10^9 Nm^2$. The wheel is subjected to a constant vertical force $F^2 = -600{,}000N$ (see Figure 6.0,

$F^1 = T = 0$). The magnitude of this force is about 20 times that of the weight of the wheel (acceleration of gravity $9.81 m/s^2$). The maximum mid-span static deflection corresponding to this load is $0.1728m$ or about $L/140$.

The lowest flexural frequency is $2.44Hz$; the lowest axial frequency is $20.8Hz$. The following initial conditions are considered: $Y^1(0) = 0$, $\mathbf{u}(S,0) = \mathbf{u}_{,t}(S,0) \equiv 0$. The wheel motion is driven mainly by its initial velocity $\dot{Y}^1(0)$. Four values of initial velocities — $1m/s$, $10m/s$, and $100m/s$† — are chosen to study the effects of complete vehicle/structure interaction, and to verify the robustness of the proposed numerical algorithms. Often, the non-dimensional quantity

$$\alpha = \frac{\dot{Y}^1}{2 f_1^2 L}, \tag{6.2}$$

where f_1^2 is the lowest flexural frequency of a beam of length L, is used to describe the dynamic character of moving load problems (see Frýba [1972]). In this example, the above initial velocities correspond to the values of α of 0.00854, 0.0854, and 0.854, respectively. The beam is discretized into two elements with $N^1 = 3$ and $N^2 = 4$. To integrate the motion, we used 200 time steps with respect to the traversing time on a rigid beam for each of the three cases (i.e., $24s$, $2.4s$, and $0.24s$). Thus, the time step size h takes respectively the values $0.12s$, $0.012s$, and $0.0012s$.

Nominal velocity. The time histories of nominal velocity for different initial velocities are plotted in Figures 6.1a-c. The largest increase in nominal velocity (about 400%) is obtained for the smallest initial velocity ($\dot{Y}^1(0) = 1m/s$, Figure 6.1a). As a result, the traversing time on the present flexible beam is about one third of the traversing time on a rigid beam. For an initial velocity of $10m/s$, the increase in velocity is drastically reduced to about 10% (Figure 6.1b), with an exit velocity of $9.96m/s$. Figure 6.1c clearly shows a loss in nominal velocity at the end of the traversing: An initial velocity

† Results for the initial velocity of $50m/s$ are given in Vu-Quoc & Olsson [1987,1988a].

of $100m/s$ drops by 0.7% to an exit velocity of $99.34m/s$, with a peak-to-peak variation in nominal velocity of 1.0% of the initial velocity. For $\dot{Y}^1(0) = 100m/s$, an analysis with 100 time steps, i.e., with $h = 0.0024s$, shows little difference in the results (Figure 6.1c). We will therefore use this time step size in the examples of a six-span beam below (Examples 6.3 and 6.4).

Structural deflection. Figure 6.1d shows the vertical mid-span displacement for different initial velocities, where time is normalized with respect to the traversing time on a rigid beam for each case. The dynamic magnification factor is 1.77 for $\dot{Y}^1(0) = 100m/s$. Observe the free vibration of the beam, after the traversing of the vehicle, clearly shown for $\dot{Y}^1(0) = 1m/s$.

Energy balance. The soundness of numerical algorithms depends in part on how well the computed results satisfy energy balance. The variation of the terms in the expression for energy balance (5.1), as a function of time, for an initial velocity of $10m/s$ is plotted in Figure 6.1e, where the legend "energy balance" means the left hand side of (5.1). (At this scale, the kinetic energy of the beam is too small to be well discernible, and is not plotted.)

Using Algorithm **1** throughout, the maximum offset of energy balance for $\dot{Y}^1(0) = 10m/s$ is 0.13% of the initial kinetic energy $\mathbb{K}_o$ $(= 0.225\times 10^6 kgm^2/s^2)$; this maximum offset is about 0.018% of $\mathbb{K}_o$ $(= 22.5\times 10^6 kgm^2/s^2)$ for $\dot{Y}^1(0) = 100m/s$. On the other hand, using Algorithm **2**, the maximum offset in energy balance for $\dot{Y}^1 = 100m/s$ is 0.008% of the corresponding $\mathbb{K}_o$, and occurs near the end of the traversing. Thus, the offset of energy balance in Algorithm **2** is roughly half of that produced in Algorithm **1**. This remark is also true in later examples. Algorithm **2** therefore not only reduces significantly the computational effort, but satisfies better the energy balance in comparison with Algorithm **1**.

Plotted in Figure 6.1f are both the energy balance and the wheel kinetic energy as a function of time for $\dot{Y}^1(0) = 100m/s$. The drop in nominal velocity at the exit (Figure

6.1c) induces a loss in the vehicle kinetic energy; this lost kinetic energy becomes the required energy to keep the beam in free vibration after the passage of the vehicle. This energy transfer thus effectively explains the Timoshenko paradox. One would then immediately ask how much the drop in nominal velocity (and kinetic energy) would be for a vehicle moving over a multiple-span beam structure. This situation will be considered in Example 6.3. •

Example 6.2. Growth of energy and proposed treatment. Here is an example where without the special treatment in Step 5 and Step 6 of Algorithms **1** and **2**, one could encounter an undesirable growth in the offset of energy balance. Consider a Maglev magnet with mass $M = 12{,}000kg$, and $I_w = \overline{R} = 0$. A vertical force of $F^2 = -600{,}000N$ is applied at its center of mass. The beam has the same properties as in Example 6.1. The system be driven by the initial conditions: $Y^1(0) = 0$, $\dot{Y}^1(0) = 30m/s$ ($\alpha = 0.256$), $\mathbf{u}(S,0) = \mathbf{u}_{,t}(S,0) \equiv 0$. The calculation is performed with 200 time steps of size $h = 0.004s$.

Oscillations in numerical results. The time history of the nominal velocity $\dot{Y}^1(t)$ is plotted in Figure 6.2a: The solid line is the result obtained with Algorithm **2**; the dotted line is the result obtained if we do not reset the axial velocity and acceleration (Steps 5 and 6), and use (4.3a) to compute both the axial velocity and the transverse velocity. Oscillations in the dotted line appear very early, with increasing amplitude compared to the smoothness of the solid line. This oscillatory pattern is even more pronounced in the time history of of energy balance (Figure 6.2b). We note that oscillations also appear when using Algorithm **1**, but with somewhat smaller amplitude, if the special treatment in Steps 5 and 6 is absent. The proposed algorithms therefore effectively remove undesirable oscillations that may occur in the results. Offset in energy balance for Algorithm **2** (solid line in Figure 6.2b) is less than 0.0013% of the initial kinetic energy K_o ($= 5.4\times 10^6 kgm^2/s^2$). This offset is 0.0026% for Algorithm **1**, in agreement with our remark in the previous example.

Source of oscillations. The mechanism triggering the aforementioned oscillatory phenomenon can be explained by looking at the equations of motion (2.5) and (2.7), recalling that $I_w = \bar{R} \equiv 0$. In particular, consider the axial acceleration $u^1{}_{,tt}$. This acceleration can be viewed as a driving force for the nominal motion, and is related to $\ddot{Y}^1$ by equation (2.5a). On the other hand, the nominal acceleration $\ddot{Y}^1$ appears on both side of equations (2.7), and play the role of a time-varying coefficient in the predictor stage. The numerical error acquired when solving for the predicted structural motion u^α is then fed back to the nominal motion through the axial acceleration $u^1{}_{,tt}$ in equation (2.5a). Depending on the initial velocity $\dot{Y}^1(0)$, this error could accumulate quickly and grow in amplitude to create the observed oscillations. Moreover, oscillations arise more noticeably for a larger ratio $M/A_\rho L$.

Finally, we note that parameters in the model could play a role in "dampening out" these oscillations: For instance, the case where the term I_w/R^2 in (2.5e) is non-zero (positive). Then the error fed back has diminishing influence on the vehicle motion — more so with larger value of I_w/R^2. It should be noticed that this type of energy growth does not occur to the transverse displacement u^2 for a similar reason: the presence of the factor $u^2{}_{,S} << 1$ of $u^2{}_{,tt}$ (see (2.5b)) as a "dampening" factor. In general, however, the proposed treatment of the axial acceleration during the predictor stage is an efficient way to eliminate oscillations. •

Example 6.3. High-speed vehicle on a six-span guideway: Energy transfer. The purpose of this example is to show the effect of vehicle/structure interaction on a long guideway, and the transfer of kinetic energy from the vehicle to the structure. We consider here a similar situation as in Example 6.1, except that the structure is a six-span continuous beam, each span of $L = 24m$ (Figure 6.0, $T = 0$). Other parameters of the model are identical to those in Example 6.1, except that here $\bar{R} = 0$. The maximum static deflection is reduced from $L/140$ to about $L/200$. The boundary conditions here are such that $u^1(0,t) = u^2(kL,t) = 0$ for $k = 0,1,...,6$, and $u^1{}_{,S}(6L,t) = u^2{}_{,SS}(0,t) =$

$u^2{}_{,SS}(6L,t) = 0$. Each span of the beam is modeled by one element of the type $(N^1, N^2) = (3,3)$, which allows discontinuity of $u^2{}_{,SSS}$ (related to shear force) at the supports. The initial velocity is set to $\dot{Y}^1(0) = 100m/s$. From experience in Example 6.1, we use 600 time steps (or 100 steps per span) to cover the traversing time on rigid guideway of $1.44s$, i.e., $h = 0.0024s$.

Nominal velocity. The vehicle nominal velocity drops steadily to a significant amount (Figure 6.3a). At the exit, this drop is about 3.5% of the initial velocity. Also, the computed nominal velocity with the present discretization differs little from that obtained with a finer space-time discretization (two elements per span, and $h = 0.0012s$), as seen from Figure 6.3a.

Energy balance. Observe the drop in nominal velocity in Figure 6.3b, as the wheel kinetic energy, with a loss of about 6.3% of its initial value, is transferred to the structure. In Algorithm **2**, the offset in energy balance is less than 0.018% of the initial kinetic energy $\mathcal{K}_o$ $(= 22.5\times 10^6 kgm^2/s^2)$; this offset is about 0.031% of $\mathcal{K}_o$ for Algorithm **1**. It is interesting to note that if the guideway (a multiple-span structure, but not necessarily continuous) is sufficiently long, a vehicle moving under its initial speed and its own weight, without any other external force, will experience a continuous drop in speed due to energy transfer, even in the absence of any energy-dissipative mechanism such as mechanical friction or aerodynamic drag.

Influence lines. Dynamic influence lines at mid-span (beam mid-span deflection vs. vehicle nominal position) are given in Figure 6.3c for the first span, and in Figure 6.3d for the last span, together with the corresponding static influence lines. In the first span, there is a characteristic delay in the dynamic response at the beginning, and a sustained motion toward the end of the traversing, instead of a "motion" whose amplitude dies out quickly as in the static case (Figure 6.3c). In the sixth span, on the other hand, the response begins to build up quickly, with increasing amplitude, as soon as the vehicle enters the third span (Figure 6.3d). This amplitude build-up could be explained by the

fact that the initial value of $\alpha = 0.854$ is close to the critical value of 1.† However, as noted above, for a sufficiently long continuous guideway and without the aid of any other external force, this amplitude growth in structural motion could not become unbounded because of the continuing loss in vehicle kinetic energy.

Contact force. We have in this example a case where the contact force $|F_c^2|$ reaches 2.5 times the vertical force $|F^2|$ (Figure 6.3e). Again, this points to the importance of the inertia term $M\ddot{u}^2$, and therefore the nonlinear term $Mu^2{}_{,S}\ddot{u}^2$, which must be retained if the equation for nominal motion (2.5) is to be valid at high speed, as noted in Remark 2.1. The horizontal contact force F_c^1, has a maximum value of about 10% of the vertical force $|F^2|$ (see Vu-Quoc & Olsson [1987]).

Example 6.4. Effects of braking on vehicle/structure system. The same model parameters as those in Example 6.3 are used here, except $\overline{R} = 0.9m$. We now consider the effects of applying the following braking torque

$$T(t) = \begin{cases} -27{,}000t \ \ (Nm) & \text{for } \ t \in [0,\ 0.1] \\ -2{,}700 \ \ \ (Nm) & \text{for } \ t > 0.1s \end{cases} \tag{6.3}$$

to the wheel (Figure 6.0). On a rigid structure, the full torque creates a deceleration of $2m/s^2$. References on analysis of braking effects of vehicles on bridge structures can be found, e.g., in Gupta & Traill-Nash [1980], and Lex-Mulcahy [1983]. Note that the vehicle models in these references have no mass in direct contact with the structure, and hence are simpler to handle. Application of a braking torque is, however, not possible in these models.

Nominal velocity. Results are given for two initial velocities: $50m/s$ and $100m/s$.‡ From Figures 6.4a-b, one observes the more pronounced effects of structure flexibility with high vehicle speed, as compared with the case of braking on a rigid structure. For

† For this type of resonance, we refer to Smith, Gilchrist & Wormley [1975] where the case of a moving force with constant speed is studied.

‡ See Vu-Quoc & Olsson [1987] for the case with initial velocity at $75m/s$.

the case with $\dot{Y}^1(0) = 50m/s$, the nominal velocity follows more or less that obtained on a rigid structure (Figure 6.4a). By contrast, the case with $\dot{Y}^1(0) = 100m/s$ leads to a significant difference in the results (Figure 6.4b). Compared with the drop in velocity at exit of a rigid structure, the structure flexibility induces an additional drop of about 7% for $\dot{Y}^1(0) = 50m/s$ (Figure 6.4a), and a sharply larger amount of 140% for $\dot{Y}^1(0) = 100m/s$ (Figure 6.4b: The exit velocity is $93.4m/s$ on flexible structure, compared with $97.2m/s$ on rigid structure). We note that, in traditional analysis of vehicle/structure interaction, the prescribed nominal velocity would coincide with the vehicle velocity on a rigid structure.

Contact force. Had we prescribed the vehicle nominal motion to be the same as that on a rigid structure, this would result in a drastic difference in the magnitude of horizontal contact force. Compare Figure 6.4c, obtained with unknown nominal motion, to Figure 6.4d, obtained with prescribed nominal motion, for $\dot{Y}^1(0) = 100m/s$.† These figures are plotted at different scales to reveal the shifting pattern of the average contact force in Figure 6.4c, as a result of complete vehicle/structure interaction at high speed. For lower speed, for example at $\dot{Y}^1(0) = 50m/s$, this contact force does not depart significantly from the case of traversing a rigid structure. The reason for the much larger horizontal contact force in the prescribed nominal motion case (3 to 4 times the contact force for unknown nominal motion) is due to the extra constraint forces that must be applied on the vehicle to make it follow the prescribed motion. •

7. Closure

We have presented an efficient and reliable computational procedure for analysis of complete vehicle/structure interaction valid for high speed regimes. In semi-discrete form, the equations of motion for the basic interaction model are not ODE's, but DAE's.

† See Vu-Quoc & Olsson [1987] for the case with initial velocity at $75m/s$.

The proposed algorithms, carrying special features pertaining to our formulation of the interaction problem, combine as sub-algorithms efficient integration methods in vehicle dynamics and in structural dynamics into global predictor/corrector algorithms. The association of highly accurate, but conditionally stable sub-algorithms to unconditionally stable sub-algorithms yields a desirable robustness in these predictor/corrector schemes.

Several examples are presented to illustrate the proposed approach. Discrete energy balance check, monitoring the numerical results, testifies to the reliability of these results, and therefore the viability of the method. We have shown some significant differences in the results, compared to those obtained in an analysis where vehicle nominal motion is prescribed. Further, energy transfer from the traversing vehicle to the supporting structure — decrease in vehicle kinetic energy, increase in energy stored in the structure, and balance of system energy — is clearly demonstrated. We thus effectively resolve the Timoshenko paradox in the spirit of Maunder [1960].

The present basic model is applicable to both wheel-on-rail and Maglev vehicles, and serves as a building block for general vehicle/structure models — an example is discussed in Vu-Quoc & Olsson [1988b]. The proposed numerical integration algorithms are not restricted to the basic model, but are also applicable to general vehicle models. As a whole, the methodology, in addition to combining the best of both worlds, could also be easily implemented in existing vehicle dynamics programs as well as in structural dynamics programs.

Acknowledgements

We appreciate many enjoyable discussions with Dr. C. Hoff during the course of this research. The kind encouragement of Profs. R.L. Taylor, J.C. Simo, and Dr. J.E. Higgins, as well as the support from The Sweden-America Foundation to M. Olsson, are gratefully acknowledged.

References

Alscher, H., Iguchi, M., Eastham, A.R., and Boldea, I. [1983], "Non-contact suspension and propulsion technology," *Vehicle System Dynamics*, Vol. 12, pp. 259-289.

Belytschko, T. [1983], "Overview of semidiscretization," in *Computational Methods for Transient Analysis*, ed. by T. Belytschko and T.J.R. Hughes, North Holland Elsevier Science Publishers, Amsterdam.

Blejwas, T.E., Feng, C.C., and Ayre, R.S. [1979], "Dynamic interaction of moving vehicles and structures," *J. Sound and Vibration*, Vol. 67, No. 4, pp. 513-521.

Butcher, J.C. [1987], *The Numerical Analysis of Ordinary Differential Equations*, John Wiley & Sons, New York.

Dalgleish, E.H., and Riches, E.E. [1986], "A review of Birmingham Maglev after one year of public service," Proc. of the *IEEE Int. Conf. on Maglev and Linear Drives*, Vanvouver, B.C., Canada, May.

Dekker, K., and Verwer, J.G. [1984], *Stability of Runge-Kutta Methods for Stiff Nonlinear Differential Equations*, CWI Monograph 2, North-Holland, Elsevier Science.

Deuflhard, P. [1985], "Recent progress in extrapolation methods for ordinary differential equations," *SIAM Review*, Vol. 27, No. 4, pp. 505-535.

Dormand, J.R., and Prince, P.J. [1978], "New Runge-Kutta algorithms for numerical simulation in dynamical astronomy," *Celestial Mechanics*, Vol. 18, pp. 223-232.

Eastham, A.R., and Hayes, W.F. [1987], "The status of development of Maglev systems," in Proc. of the *37th IEEE Vehicular Technology Conference*, Tampa, Florida, June, pp. 231-239.

Fine, J.M. [1987], "Low-order practical Runge-Kutta-Nyström methods," *Computing*, Vol. 38, pp. 281-297.

Frýba, L. [1972], *Vibration of Solids and Structures under Moving Loads*, Noordhoff International Publishing, Groningen.

Führer, C. [1986], "Numerical integration methods in vehicle dynamics simulation," Proc. of the *3rd ICTS Course and Seminar on Advanced Vehicle System Dynamics*, Amalfi, Italy, May, pp. 329-345.

Führer, C., and Wallrapp, O. [1984], "A computer-oriented method for reducing linearized multibody system equations by incorporating constraints, *Comp. Meth. Appl. Mech. Engng.*, Vol. 46, pp. 169-175.

Gear, C.W. [1971], *Numerical Initial Value Problems in Ordinary Differential Equations*, Prentice-Hall, New York.

Gear, C.W. [1978], "The stability of numerical methods of 2nd order ODE's," *SIAM J. Numerical Analysis*, Vol. 15, pp. 188-197.

Gear, C.W. [1980], "Runge-Kutta starters for multistep methods," *ACM Transaction on Mathematical Software*, Vol. 6, pp. 263-279.

Gellert, M. [1978], "A new algorithm for integration of dynamic systems," *Computers & Structures*, Vol. 9, pp. 401-408.

Gupta, G.K. [1980], "A note about overhead costs in ODE solvers," *ACM Transaction*

on Mathematical Software, Vol. 6, No. 3, pp. 319-326.

Gupta, G.K., Sacks-Davis, R., and Tischer, P.E. [1985], "A review of recent developments in solving ODEs," *ACM Computing Surveys*, Vol. 17, No. 1, pp. 5-47.

Gupta, R.K., and Traill-Nash, R.W. [1980], "Bridge dynamic loading due to road surface irregularities and braking of vehicle," *Earthq. Engng. and Struct. Dyn.*, Vol. 8, pp. 83-96.

Hairer [1981], "Order conditions for numerical methods for partitioned ordinary differential equations," *Numer. Math.*, Vol. 36, pp. 431-445.

Hilber, H.M., Hughes, T.J.R., and Taylor, R.L. [1977], "Improved numerical dissipation for time integration algorithms in structural dynamics," *Earthq. Engng. & Struct. Dyn.*, Vol. 5, pp. 283-292.

Hoff, C. [1986], *Dissipative Step-by-Step Integration Methods for Nonlinear Structures under Earthquake Loading* (in German), Doctoral Dissertation D83, Technical University of Berlin, West Germany.

Hoff, C., and Pahl, P.J. [1987], "Development of an implicit method with numerical dissipation from a generalized single step algorithm for structural dynamics," preprint, to appear in *Comp. Meth. Appl. Mech. Engng.*

Hughes, T.J.R. [1983], "Analysis of transient algorithms with particular reference to stability behavior," in *Computational Methods for Transient Analysis*, ed. by T. Belytschko and T.J.R. Hughes, North Holland Elsevier Science Publishers, Amsterdam.

Kalker, J.J. [1979], "Survey of wheel-rail rolling contact theory," *Vehicle System Dynamics*, Vol. 5, pp. 317-358.

Katona, M.G., and Zienkiewicz, O.C. [1985], "A unified set of single step algorithms. Part 3: The beta-*m* method, a generalization of the Newmark scheme," *Int. J. Num. Meth. Engng.*, Vol. 21, pp. 1345-1359.

Kortüm, W. [1986], "Introduction to system-dynamics of ground vehicles," in Proc. of the *3rd ICTS Course and Seminar on Advanced Vehicle System Dynamics*, Amalfi, Italy, May, pp. 1-36.

Lambert, J.D. [1973], *Computational Methods in Ordinary Differential Equations*, John Wiley & Sons, London.

Lawton, A. [1985], "Implementation of a Maglev vehicle suspension for flexible guideways," in Proc. of the *9th IASVD Symposium*, Linköping University, Linköping, Sweden, pp. 293-306.

Lex-Mulcahy, N. [1983], "Bridge response with tractor-trailer vehicle loading," *Earthq. Engng. and Struct. Dyn.*, Vol. 11, pp. 649-665.

Maunder, L. [1960], "On the work of a force crossing a beam," *Quart. of Applied Mathematics*, Vol. 17, pp. 437-440.

Nikravesh, P.E. [1984], "Some methods for dynamics analysis of constrained mechanical

systems: A survey," in *Computer Aided Analysis and Optimization of Mechanical Systems*, edited by J. Haug, Springer, Berlin, pp. 351-368.

Olsson, M. [1985], "Finite element, modal co-ordinate analysis of structures subjected to moving loads," *J. Sound and Vibration*, Vol. 99, No. 1, pp. 1-12.

Olsson, M. [1986], *Analysis of Structures Subjected to Moving Loads*, Doctoral Dissertation, Report TVSM-1003, Division of Structural Mechanics, Lund University, Sweden.

Park, K.C., and Felippa, C.A. [1983], "Partitioned Analysis of Coupled Systems," in *Computational Methods for Transient Analysis*, ed. by T. Belytschko and T.J.R. Hughes, North Holland Elsevier Science Publishers, Amsterdam.

Petzold, L.R. [1982], "A description of DASSL: A differential/algebraic system solver," in Proc. of the 10th IMACS *World Congress on System Simulation and Scientific Computation*, Montreal, August.

Smith, C.C., Gilchrist, A.J., and Wormley, D.N. [1975], "Multiple and continuous span elevated guideway-vehicle dynamic performance," *ASME J. Dynamic Systems, Measurements, and Control*, Vol. 97, No. 1, pp. 30-40.

Trujillo, D.H. [1972], "An unconditionally stable explicit algorithm for structural dynamics," *Int. J. Num. Meth. Engng.*, Vol. 11, pp. 1579-1592.

Venancio-Filho, F. [1978], "Finite element analysis of structures under moving loads," *Shock and Vibration Digest*, Vol. 10, No. 8, pp. 27-35.

Vu-Quoc, L. [1986], *Dynamics of Flexible Structures Performing Large Overall Motions: A Geometrically-Nonlinear Approach*, Doctoral Dissertation, Electronics Research Laboratory Memorandum UCB/ERL M86/36, University of California, Berkeley.

Vu-Quoc, L., and Olsson, M. [1987], *Interaction between High-Speed Moving Vehicles and Flexible Structures: An Analysis without Assumption of Known Vehicle Nominal Motion*, Structural Engineering, Mechanics, and Materials, Report No. UCB/SEMM-87/10, NISEE Center, University of California, Berkeley, December.

Vu-Quoc, L., and Olsson, M. [1988a], "Formulation of a basic building-block model for interaction of high-speed vehicles on flexible structures," submitted for publication.

Vu-Quoc, L., and Olsson, M. [1988b], "Some aspects of vehicle/structure interaction for high-speed vehicles on multiple-span elevated guideways. Part I: Lumped-parameters vehicle model," in preparation.

Vu-Quoc, L., and Simo, J.C. [1988], "Dynamics of earth-orbiting satellites with flexible multibody components," to appear in *AIAA J. Guidance, Control, and Dynamics.*

Wallrapp, O. [1986], "Elastic vehicle guideway structures," in Proc. of the *3rd ICTS Course and Seminar on Advanced Vehicle System Dynamics*, Amalfi, Italy, May, pp. 215-232.

Wood, W.L. [1987], "Some transient and coupled problems — A state-of-the-art review," in *Numerical Methods for Transient and Coupled Problems*, edited by R.W. Lewis

et al, John Wiley & Sons Ltd.

Zicha, J.H. [1986], "Civil aspects of Maglev design," *IEEE Int. Conf. on Maglev & Linear Drives*, Vancouver, Canada, May, pp. 69-87.

Zienkiewicz, O.C. [1977], *The Finite Element Method*, McGraw Hill, New York.

Figure captions

Figure 1.1. Electromagnetic Maglev vehicle with magnet units ("magnetic wheels").

Figure 2.1. *Basic problem.* Model parameters.

Figure 6.0. *Basic vehicle/structure models.* Simple-span and six-span beam structures.

Figure 6.1a. *Vehicle traversing a simple-span guideway.* Nominal velocity vs. Time. Initial velocity $\dot{Y}^1(0) = 1m/s$. Beam length $L = 24m$.

Figure 6.1b. *Vehicle traversing a simple-span guideway.* Nominal velocity vs. Time. Initial velocity $\dot{Y}^1(0) = 10m/s$. Beam length $L = 24m$.

Figure 6.1c. *Vehicle traversing a simple-span guideway.* Nominal velocity vs. Time. Initial velocity $\dot{Y}^1(0) = 100m/s$. Beam length $L = 24m$. Solid line: 200 time steps. Dotted line: 100 time steps.

Figure 6.1d. *Vehicle traversing a simple-span guideway.* Vertical mid-span displacement (normalized wrt $0.1728m$) vs. Time (normalized wrt traversing time on rigid beam). $\dot{Y}^1(0) = 1m/s, 10m/s, 50m/s, 100m/s$. $L = 24m$.

Figure 6.1e. *Vehicle traversing a simple-span guideway.* Energy ($\times 10^6$) vs. Time. Initial velocity $\dot{Y}^1(0) = 10m/s$.

Figure 6.1f. *Vehicle traversing a simple-span guideway.* Energy ($\times 10^6$) vs. Time. Solid line: energy balance. Dotted line: wheel kinetic energy. Initial velocity $\dot{Y}^1(0) = 100m/s$.

Figure 6.2a. *Growth of energy and proposed treatment.* Nominal velocity vs. Time. Solid line: Algorithm **2**. Dotted line: Algorithm **2** without treatment of axial motion.

Figure 6.2b. *Growth of energy and proposed treatment.* Energy balance ($\times 10^6$) vs. Time. Solid line: Algorithm **2**. Dotted line: Algorithm **2** without treatment of axial motion.

Figure 6.3a. *High-speed vehicle on a six-span guideway.* Nominal velocity vs. Time. Solid line: 1 element per span and $h = 0.0024s$. Dotted line: 2 elements per span and $h = 0.0012s$.

Figure 6.3b. *High-speed vehicle on a six-span guideway.* Energy ($\times 10^6$) vs. Time. Solid line: energy balance. Dotted line: wheel kinetic energy.

Figure 6.3c. *High-speed vehicle on a six-span guideway.* Influence line: Vertical mid-span deflection in first span vs. Nominal position. Solid line: dynamic. Dotted line: static.

Figure 6.3d. *High-speed vehicle on a six-span guideway.* Influence line: Vertical mid-span deflection in 6th span vs. Nominal position. Solid line: dynamic. Dotted line: static.

Figure 6.3e. *High-speed vehicle on a six-span guideway.* Vertical contact force F_c^2 (normalized wrt vertical force F^2) vs. Time.

Figure 6.4a. *Effects of braking on vehicle/structure system.* Nominal velocity vs. Time. Six-span beam. Initial velocity $\dot{Y}^1(0) = 50m/s$. Solid line: flexible structure and unknown nominal motion. Dotted line: rigid structure, or flexible structure with prescribed nominal motion.

Figure 6.4b. *Effects of braking on vehicle/structure system.* Nominal velocity vs. Time. Six-span beam. Initial velocity $\dot{Y}^1(0) = 100m/s$. Solid line: flexible structure and unknown nominal motion. Dotted line: rigid structure, or flexible structure with prescribed nominal motion.

Figure 6.4c. *Effects of braking on vehicle/structure system.* Horizontal contact force F_c^1 (normalized wrt vertical force $|F^2|$) vs. Time. Solid line: flexible structure and unknown nominal motion. Dotted line: rigid structure. $\dot{Y}^1(0) = 100m/s$.

Figure 6.4d. *Effects of braking on vehicle/structure system.* Horizontal contact force F_c^1 (normalized wrt vertical force $|F^2|$) vs. Time. Solid line: flexible structure and prescribed nominal motion. Dotted line: rigid structure. $\dot{Y}^1(0) = 100m/s$.

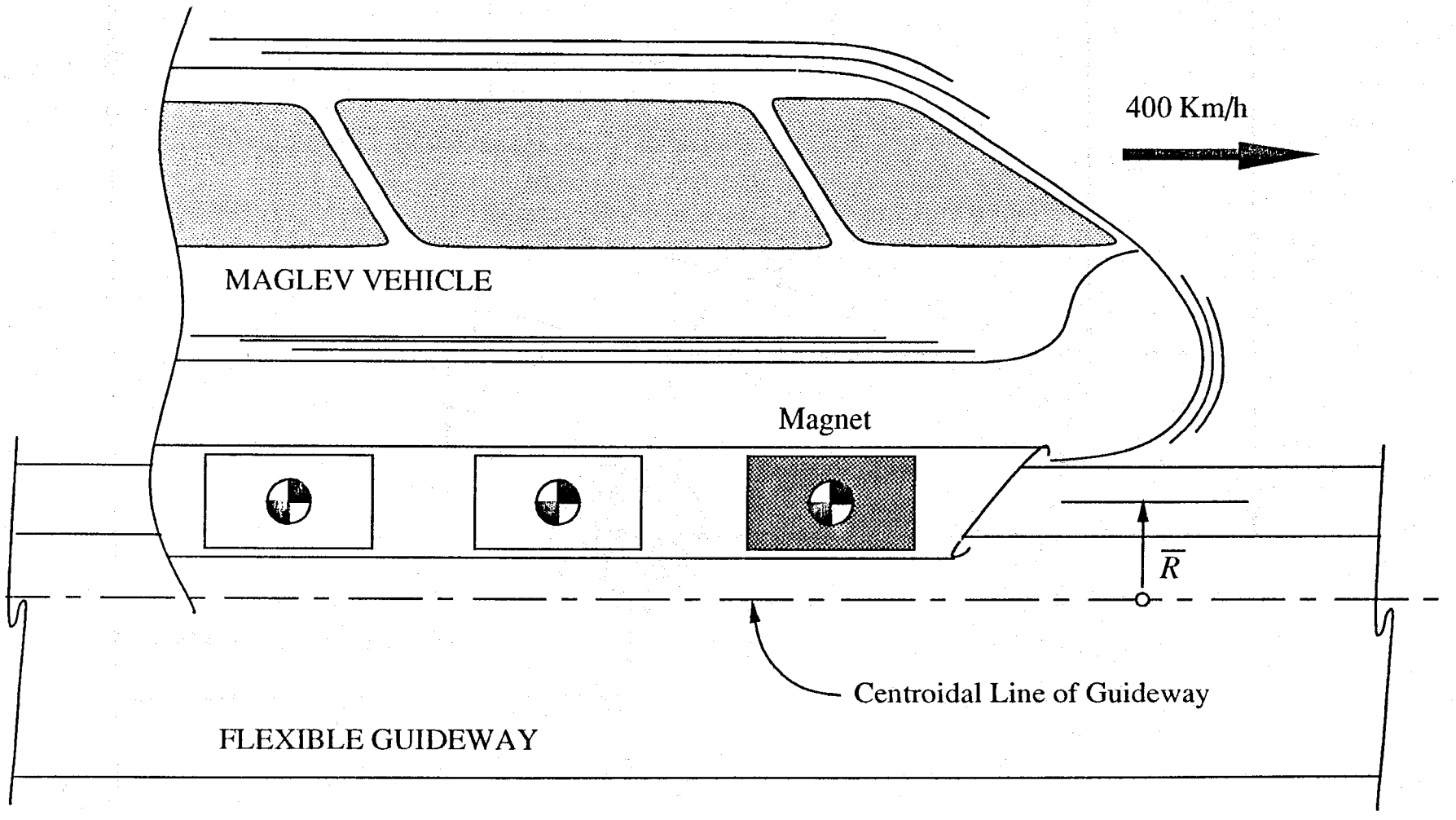

Figure 1.1. Electromagnetic Maglev vehicle with magnet units ("magnetic wheels").

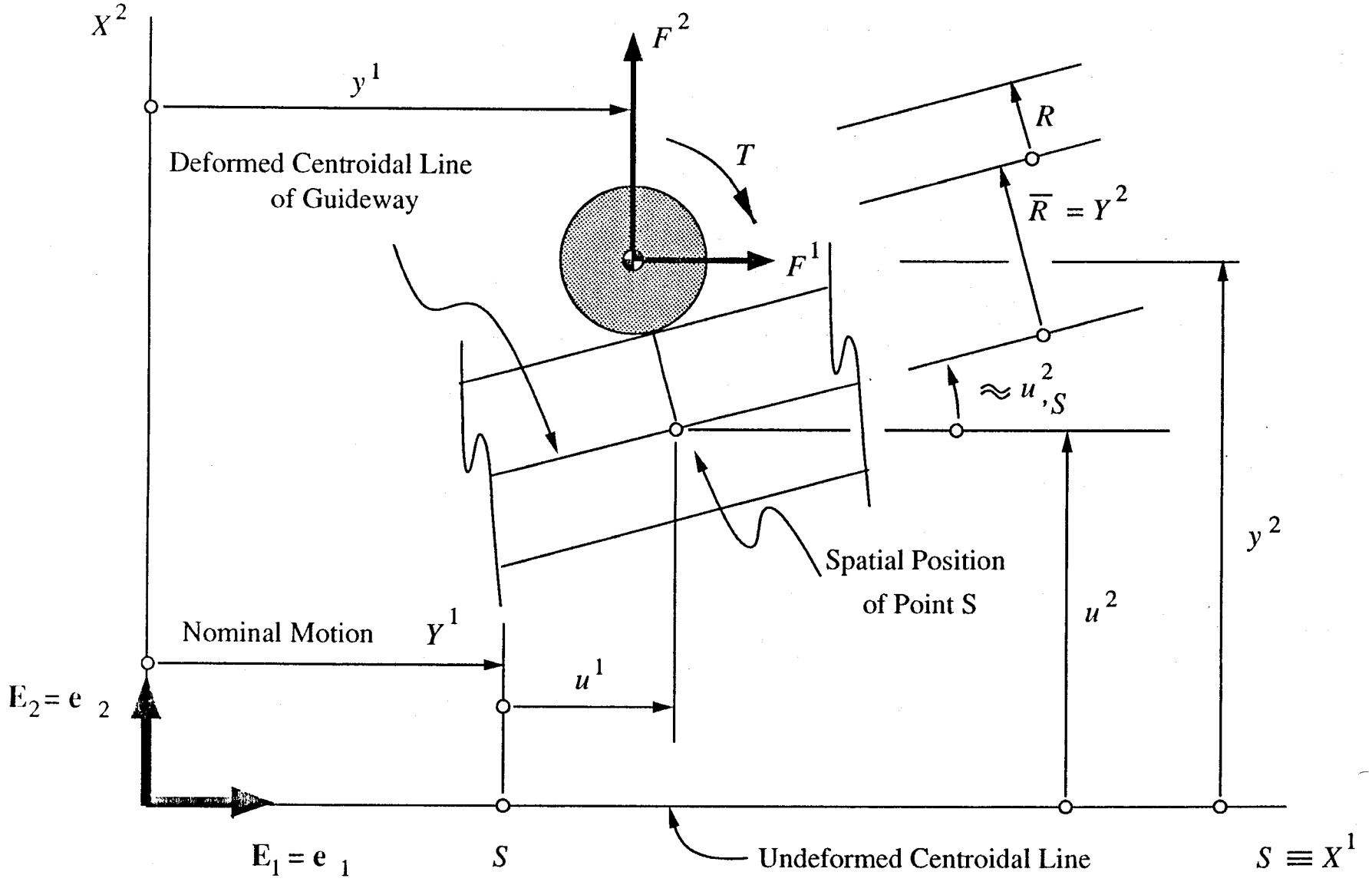

Figure 2.1. *Basic problem.* Model parameters.

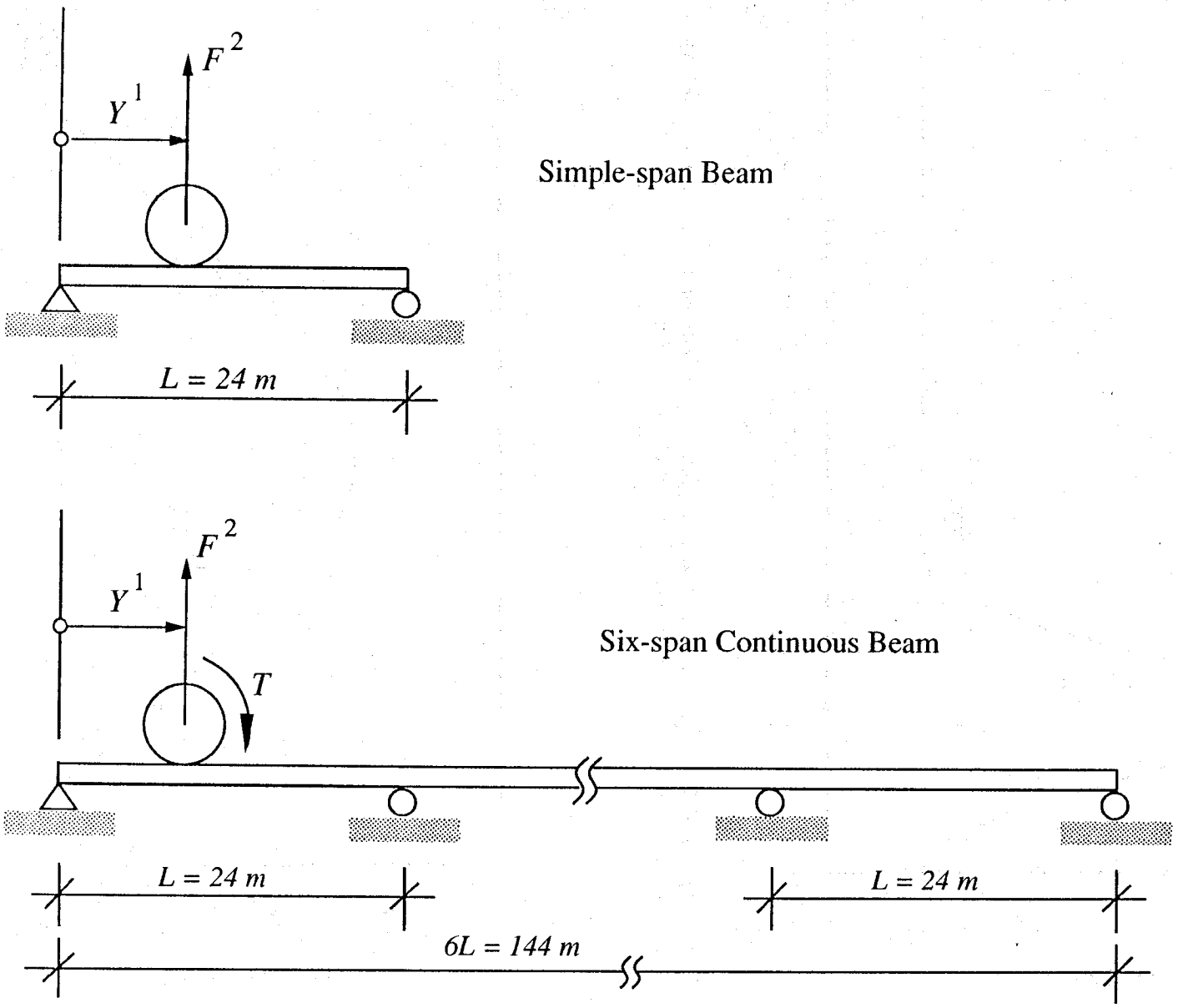

Figure 6.0. *Basic vehicle/structure models.* Simple-span and six-span beam structures.

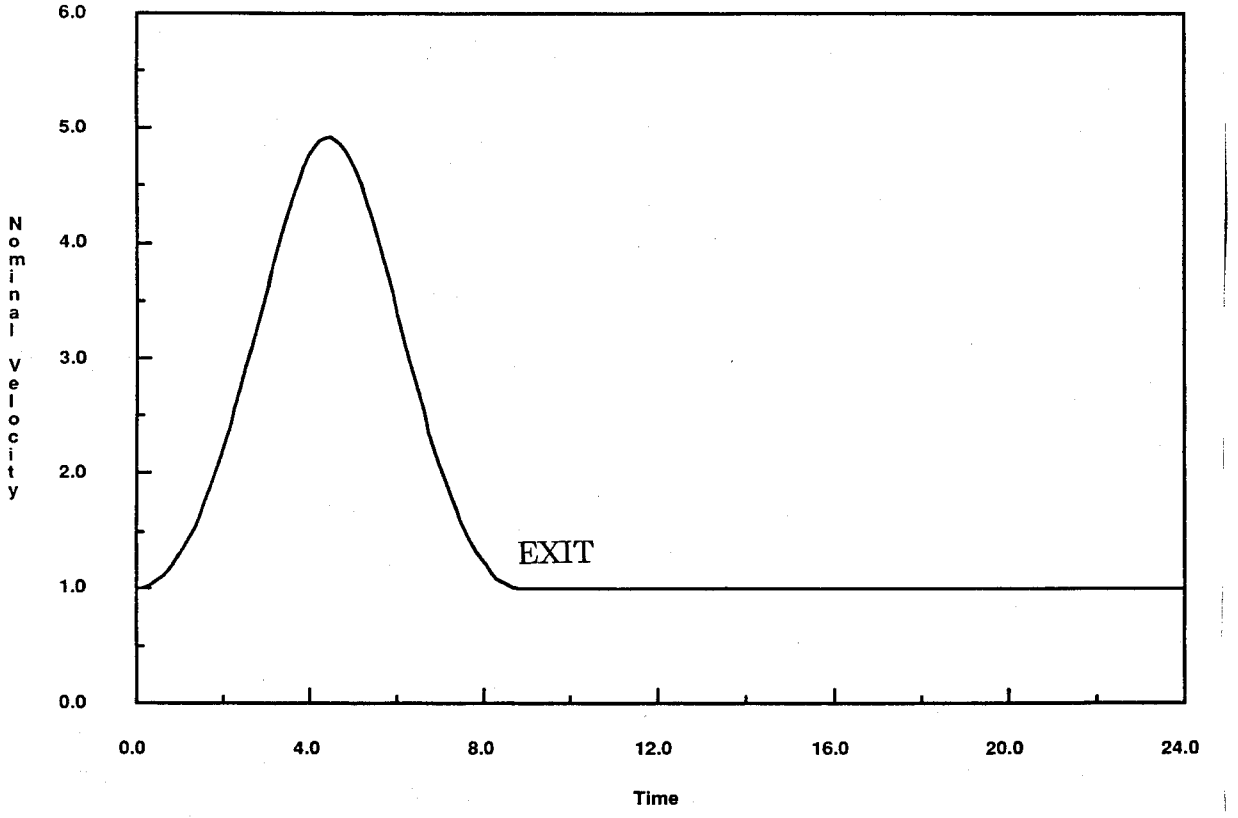

Figure 6.1a. *Vehicle traversing a simple-span guideway.* Nominal velocity vs. Time. Initial velocity $\dot{Y}^1(0) = 1m/s$. Beam length $L = 24m$.

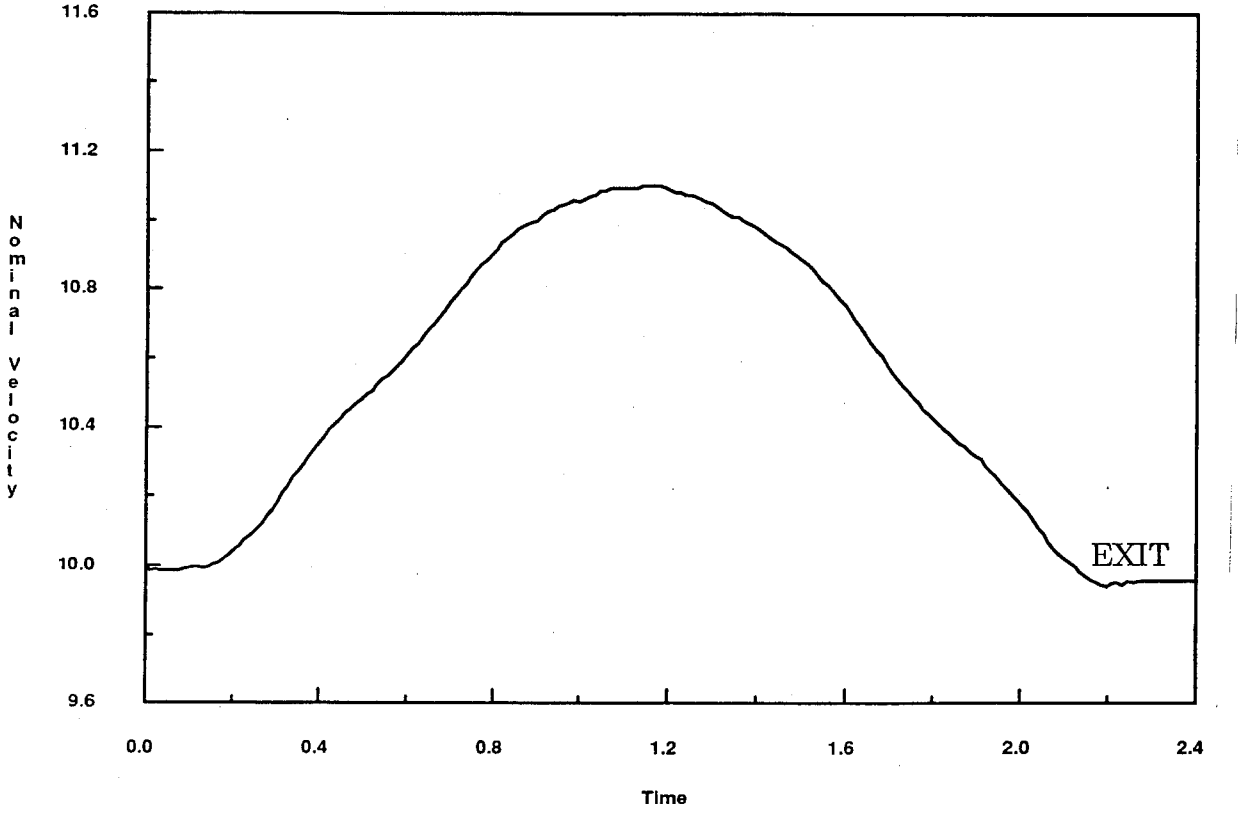

Figure 6.1b. *Vehicle traversing a simple-span guideway.* Nominal velocity vs. Time. Initial velocity $\dot{Y}^1(0) = 10m/s$. Beam length $L = 24m$.

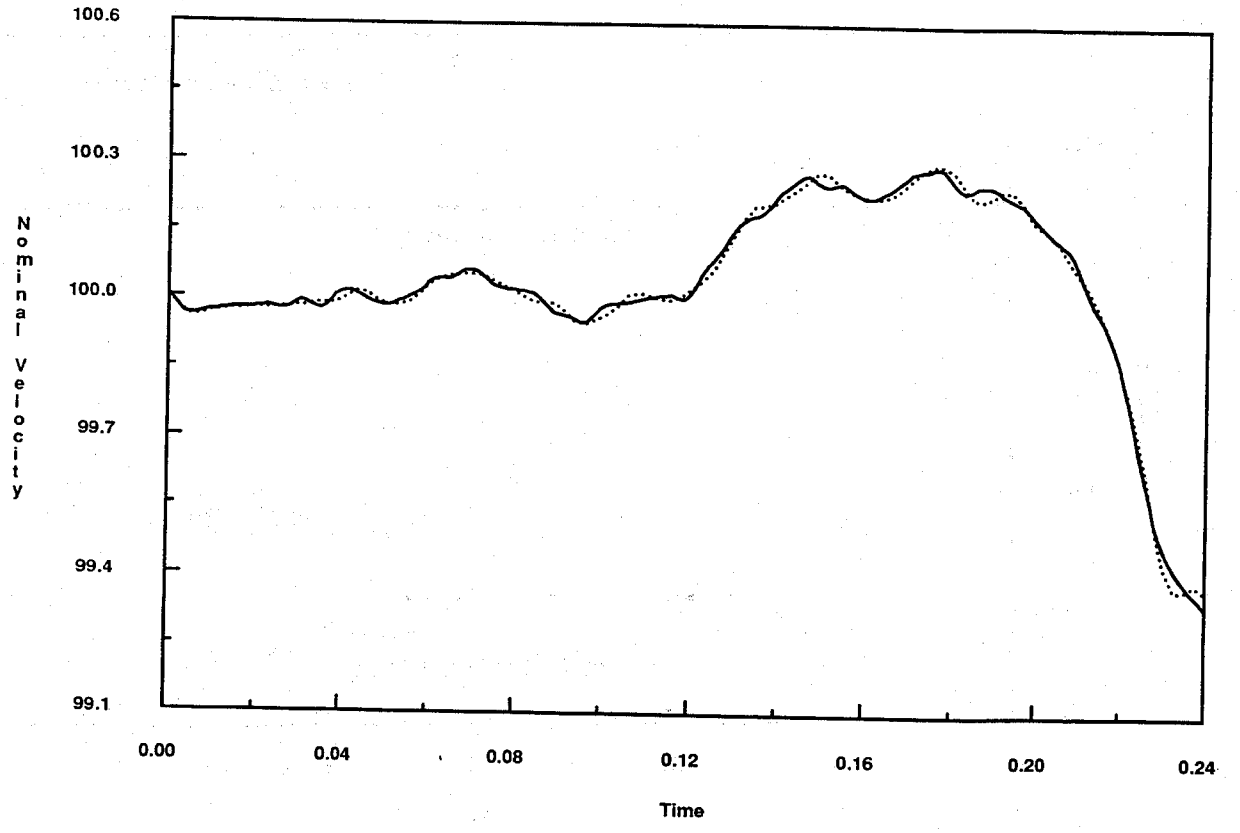

Figure 6.1c. *Vehicle traversing a simple-span guideway.* Nominal velocity vs. Time. Initial velocity $\dot{Y}^1(0) = 100m/s$. Beam length $L = 24m$. Solid line: 200 time steps. Dotted line: 100 time steps.

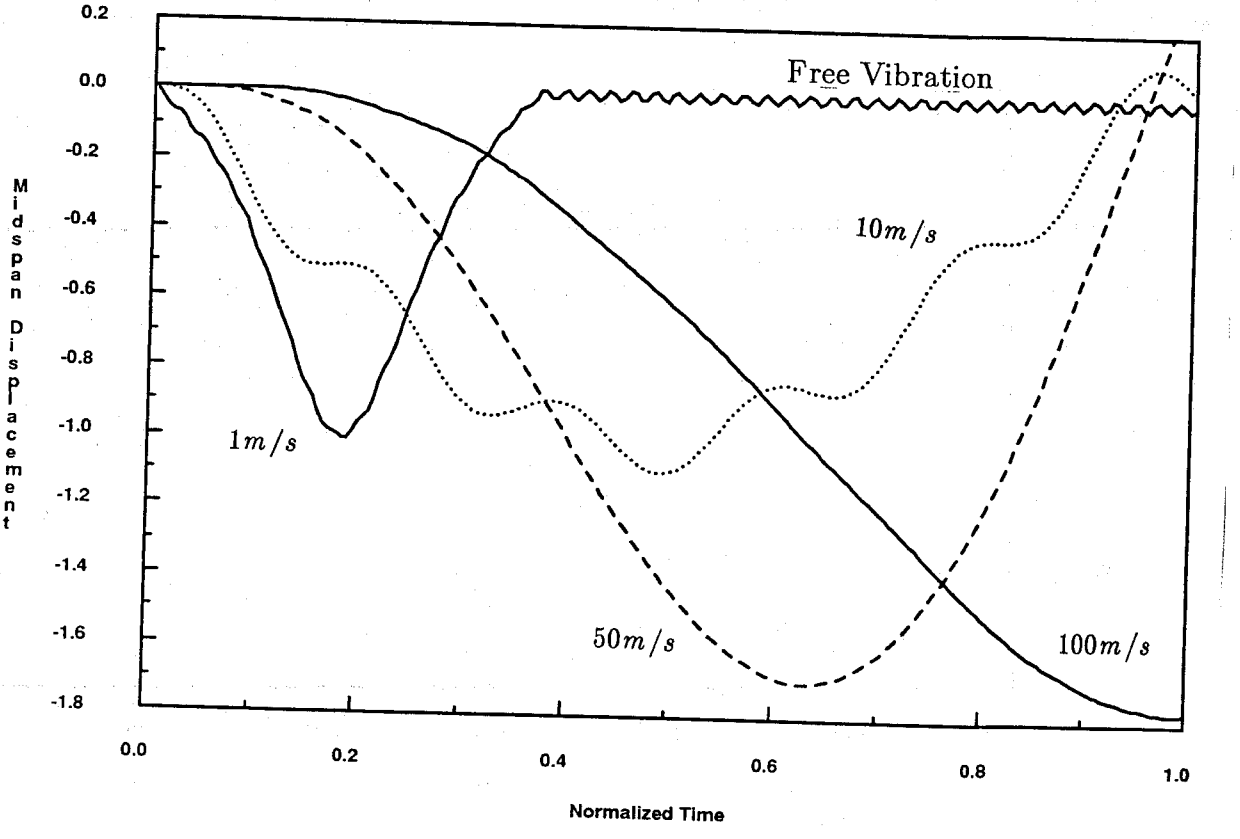

Figure 6.1d. *Vehicle traversing a simple-span guideway.* Vertical mid-span displacement (normalized wrt $0.1728m$) vs. Time (normalized wrt traversing time on rigid beam). $\dot{Y}^1(0) = 1m/s, 10m/s, 50m/s, 100m/s$. $L = 24m$.

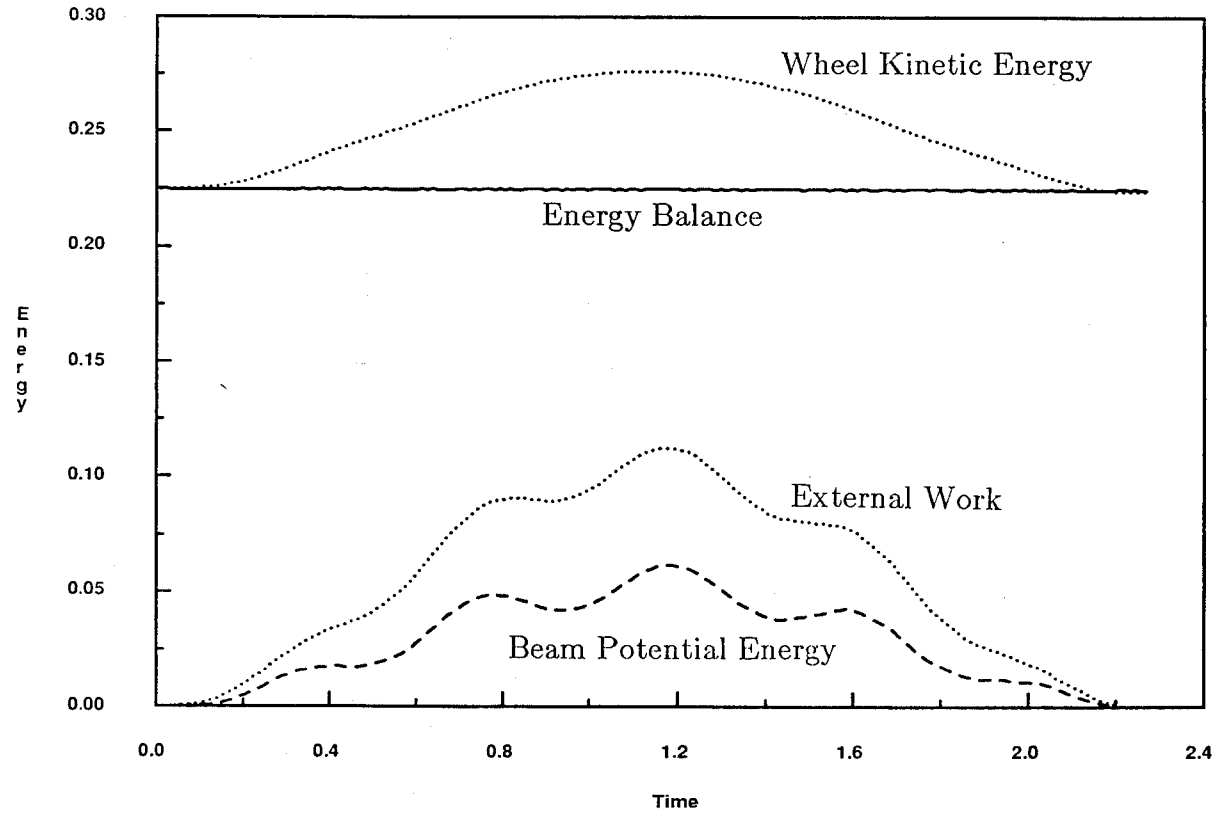

Figure 6.1e. *Vehicle traversing a simple-span guideway.* Energy ($\times 10^6$) vs. Time. Initial velocity $\dot{Y}^1(0) = 10m/s$.

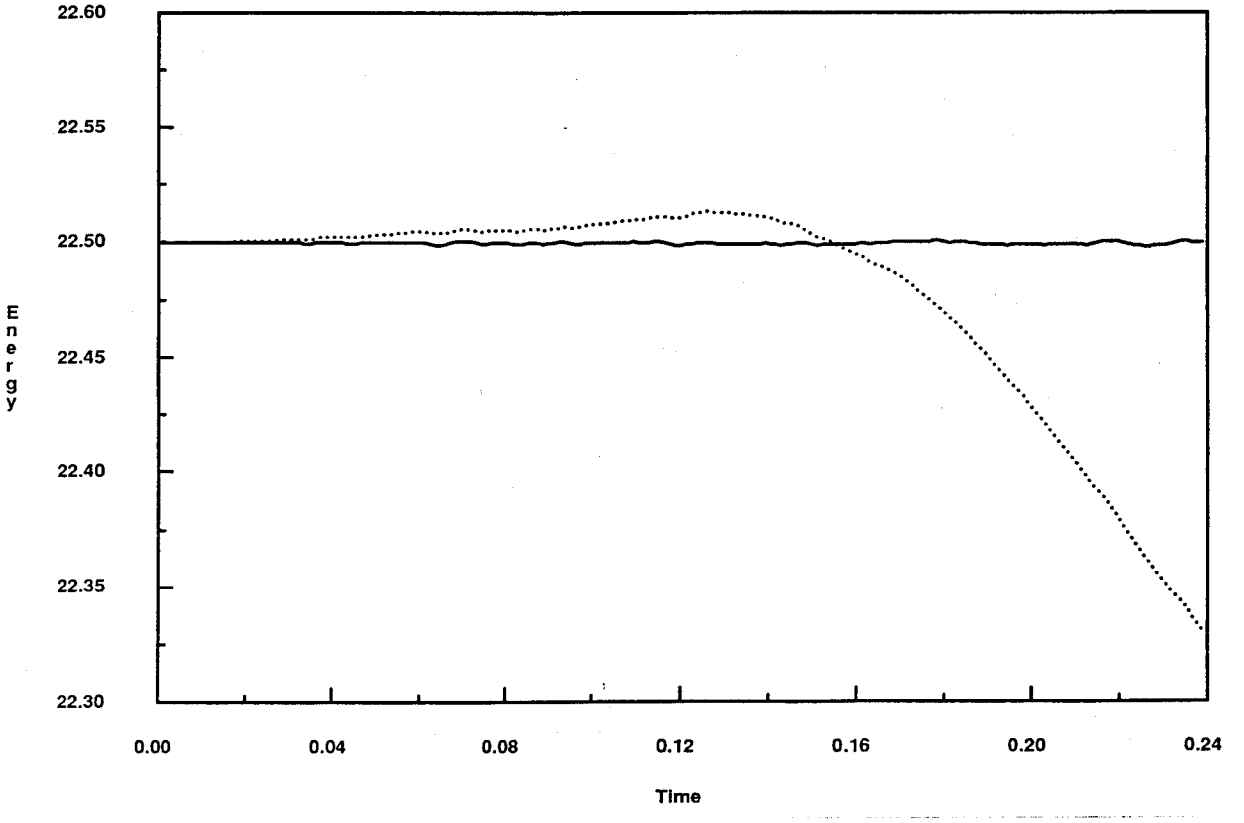

Figure 6.1f. *Vehicle traversing a simple-span guideway.* Energy ($\times 10^6$) vs. Time. Solid line: energy balance. Dotted line: wheel kinetic energy. Initial velocity $\dot{Y}^1(0) = 100m/s$.

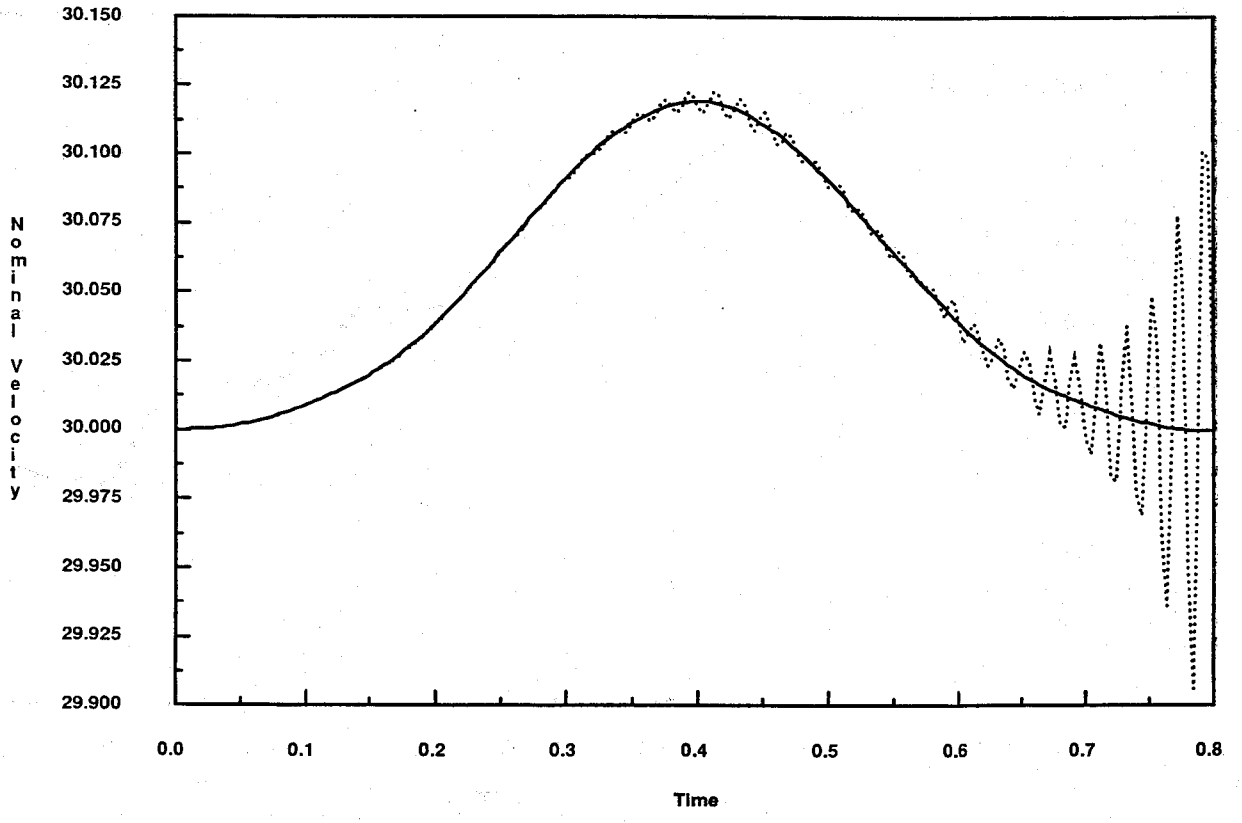

Figure 6.2a. *Growth of energy and proposed treatment.* Nominal velocity vs. Time. Solid line: Algorithm **2**. Dotted line: Algorithm **2** without treatment of axial motion.

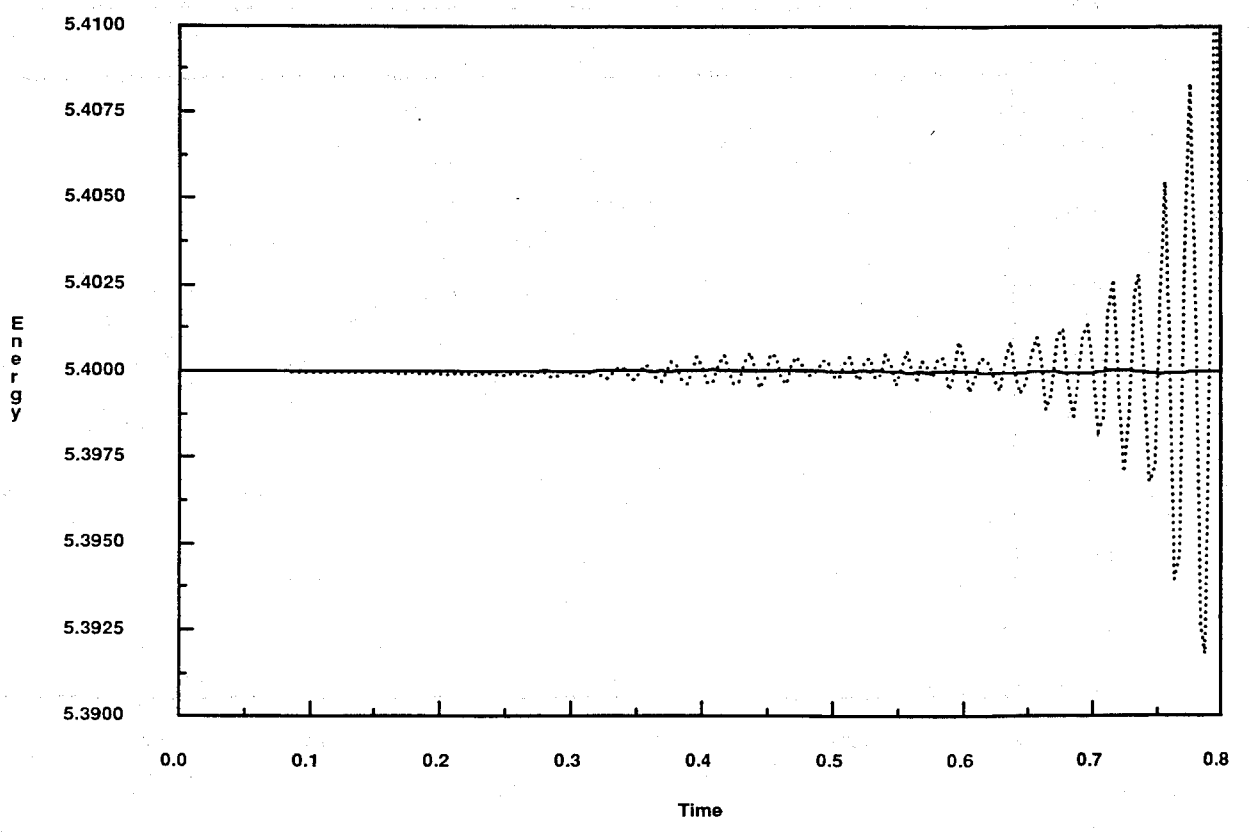

Figure 6.2b. *Growth of energy and proposed treatment.* Energy balance ($\times 10^6$) vs. Time. Solid line: Algorithm **2**. Dotted line: Algorithm **2** without treatment of axial motion.

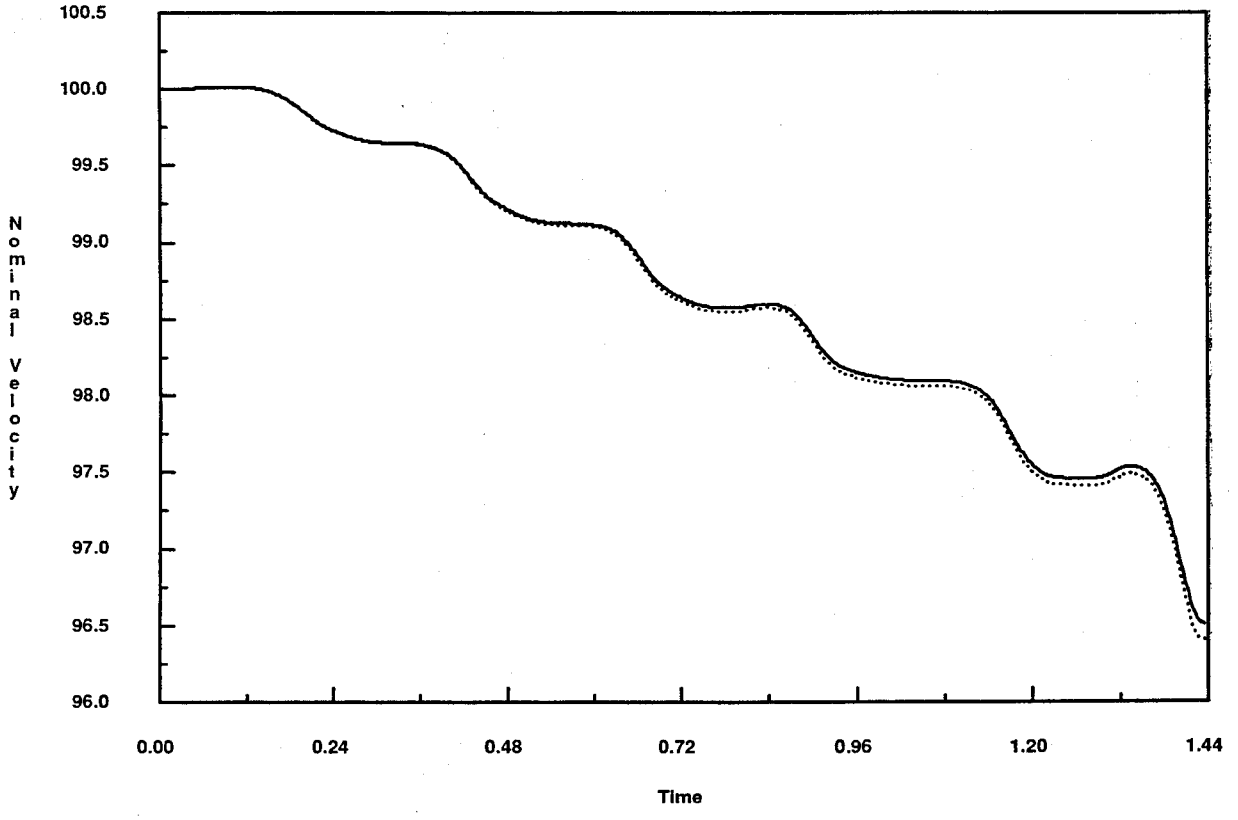

Figure 6.3a. *High-speed vehicle on a six-span guideway.* Nominal velocity vs. Time. Solid line: 1 element per span and $h = 0.0024s$. Dotted line: 2 elements per span and $h = 0.0012s$.

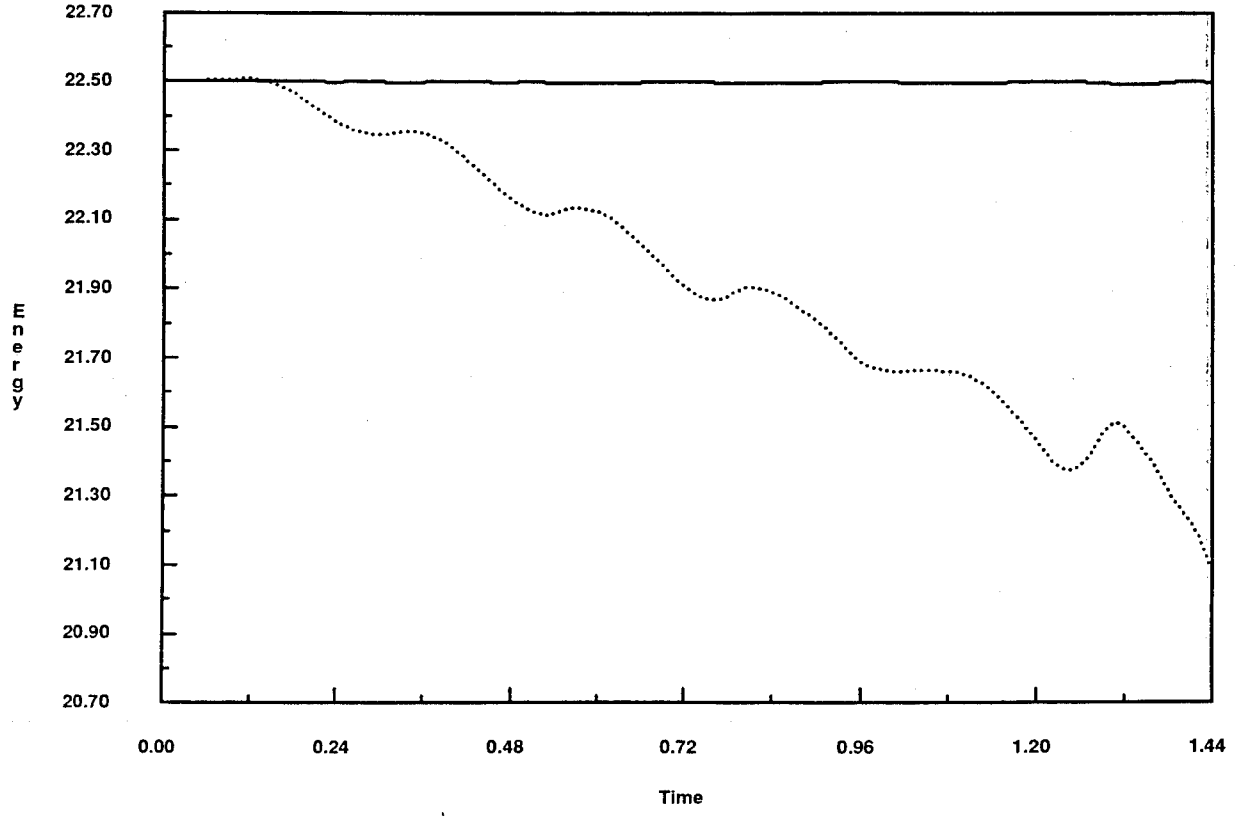

Figure 6.3b. *High-speed vehicle on a six-span guideway.* Energy ($\times 10^6$) vs. Time. Solid line: energy balance. Dotted line: wheel kinetic energy.

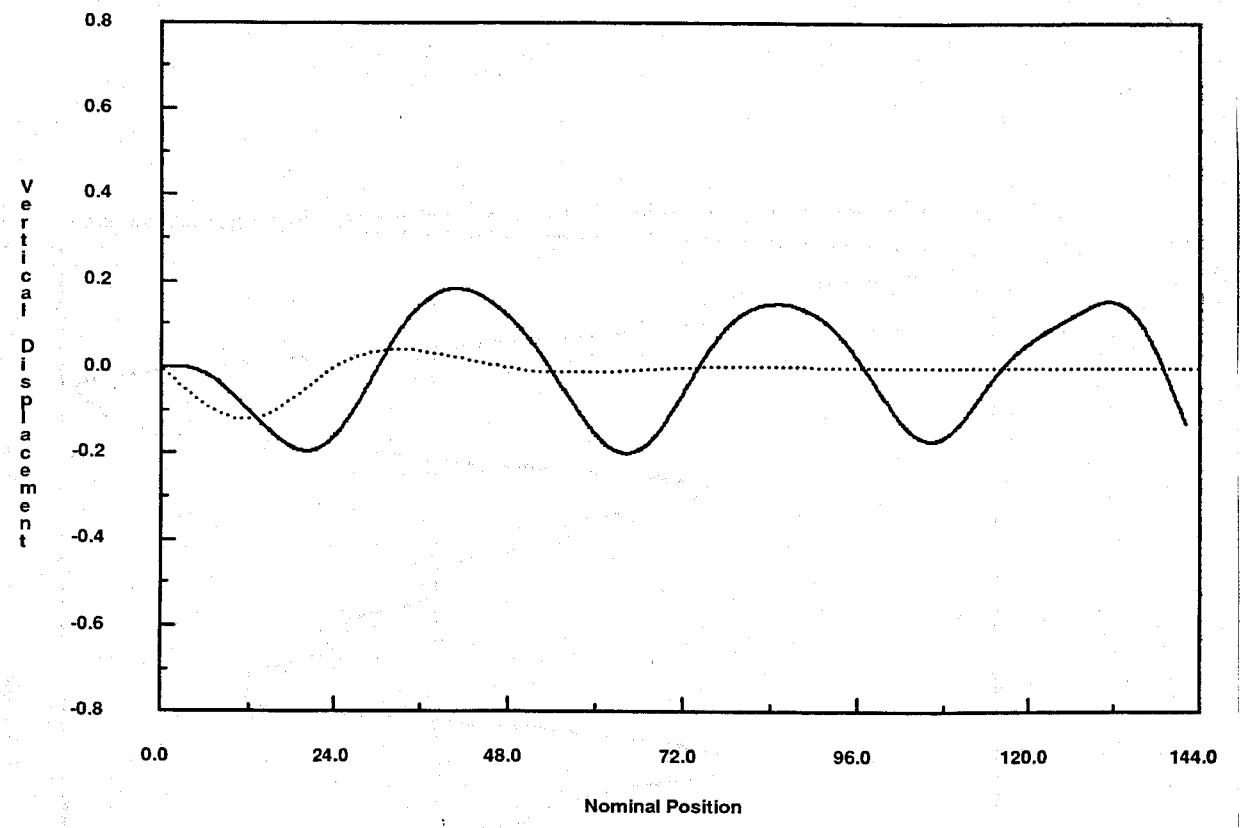

Figure 6.3c. *High-speed vehicle on a six-span guideway.* Influence line: Vertical mid-span deflection in first span vs. Nominal position. Solid line: dynamic. Dotted line: static.

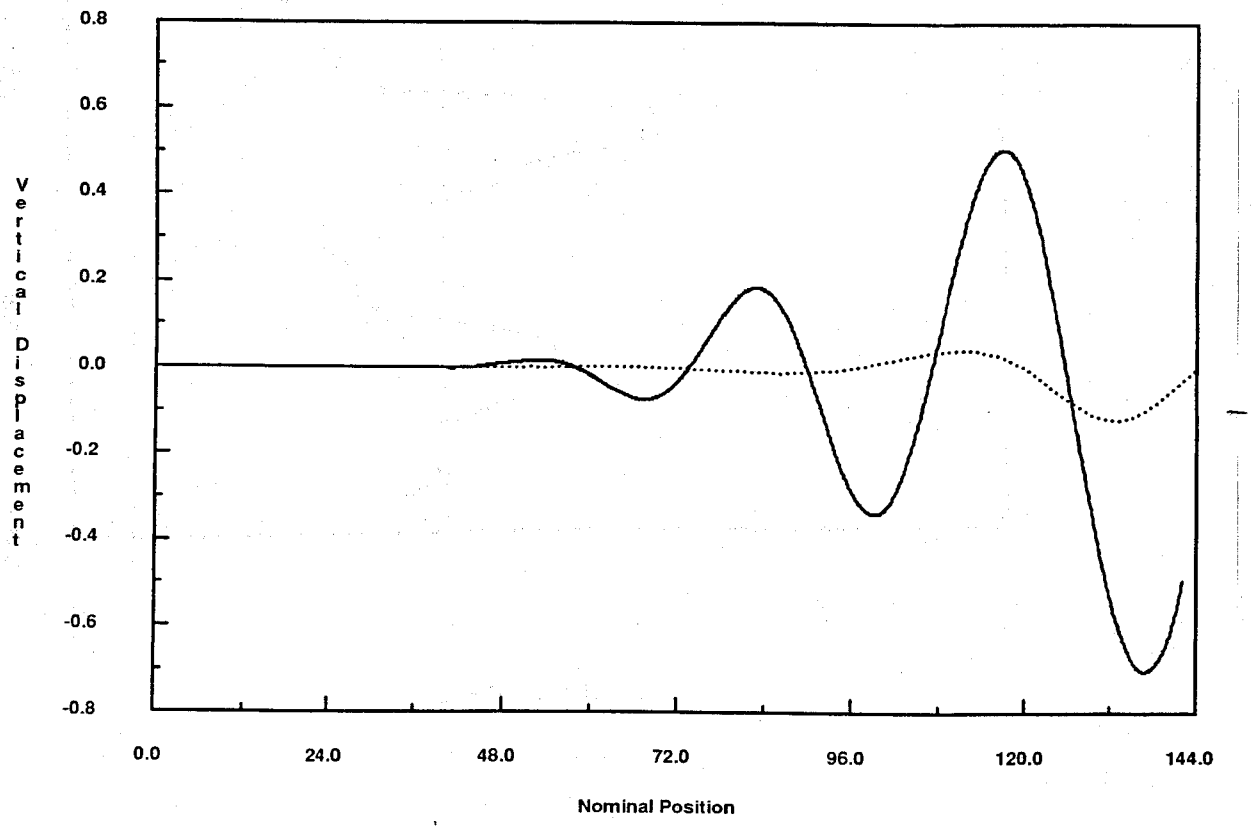

Figure 6.3d. *High-speed vehicle on a six-span guideway.* Influence line: Vertical mid-span deflection in 6th span vs. Nominal position. Solid line: dynamic. Dotted line: static.

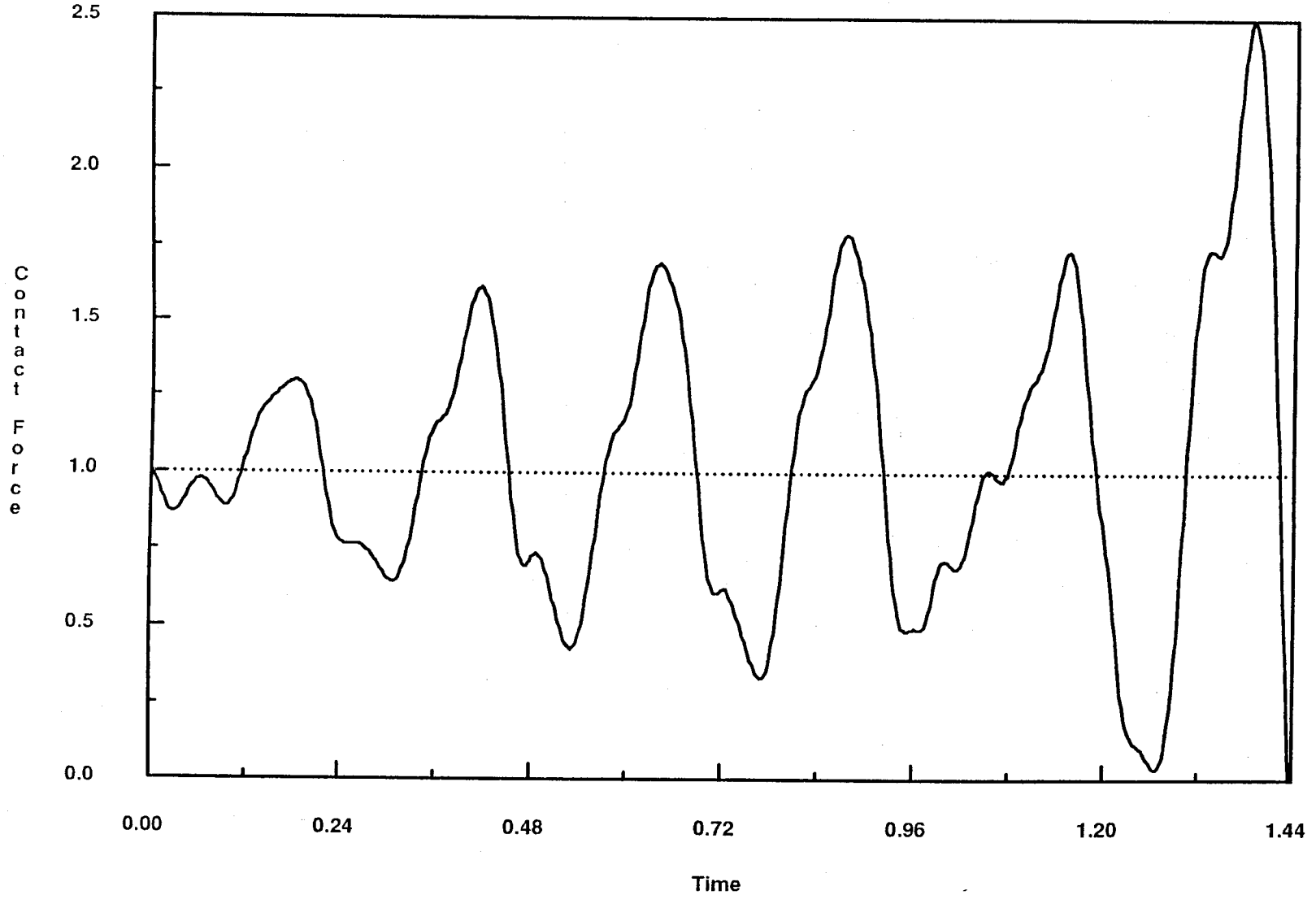

Figure 6.3e. *High-speed vehicle on a six-span guideway.* Vertical contact force F_c^2 (normalized wrt vertical force F^2) vs. Time.

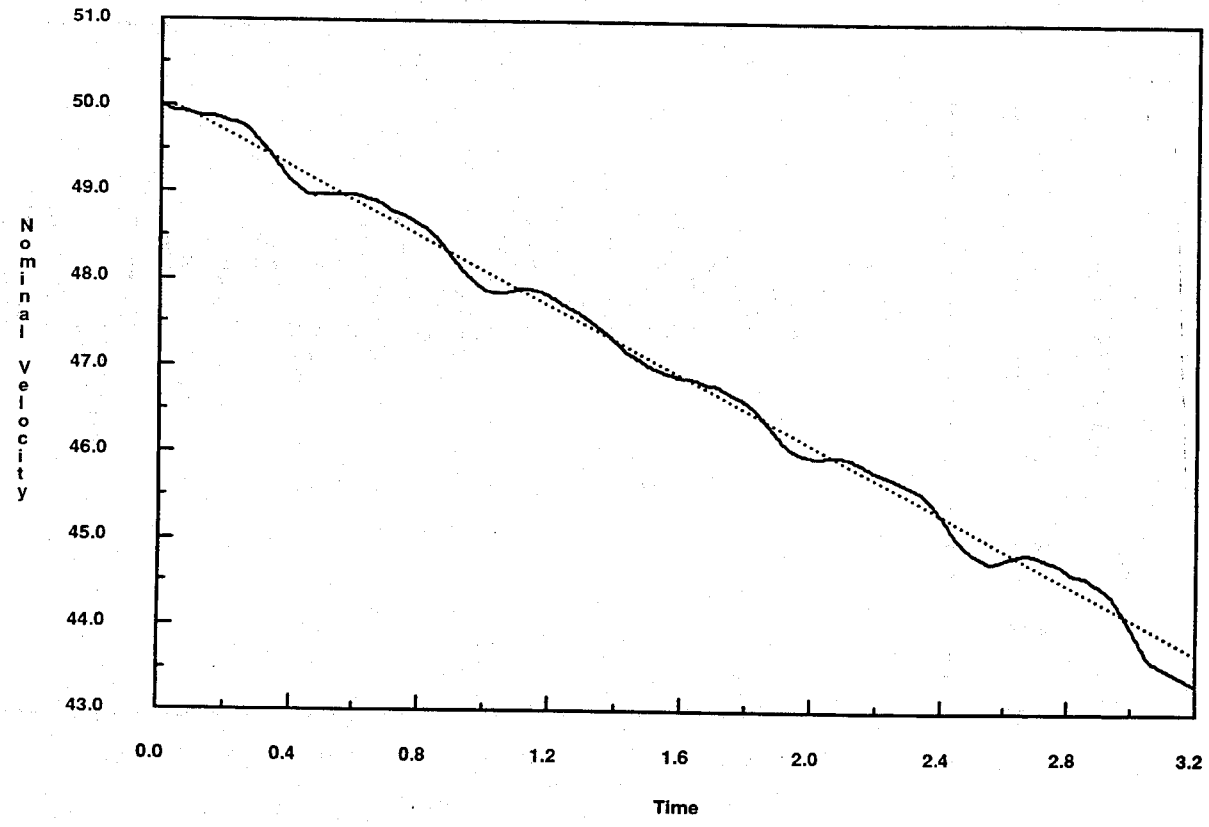

Figure 6.4a. *Effects of braking on vehicle/structure system.* Nominal velocity vs. Time. Six-span beam. Initial velocity $\dot{Y}^1(0) = 50m/s$. Solid line: flexible structure and unknown nominal motion. Dotted line: rigid structure, or flexible structure with prescribed nominal motion.

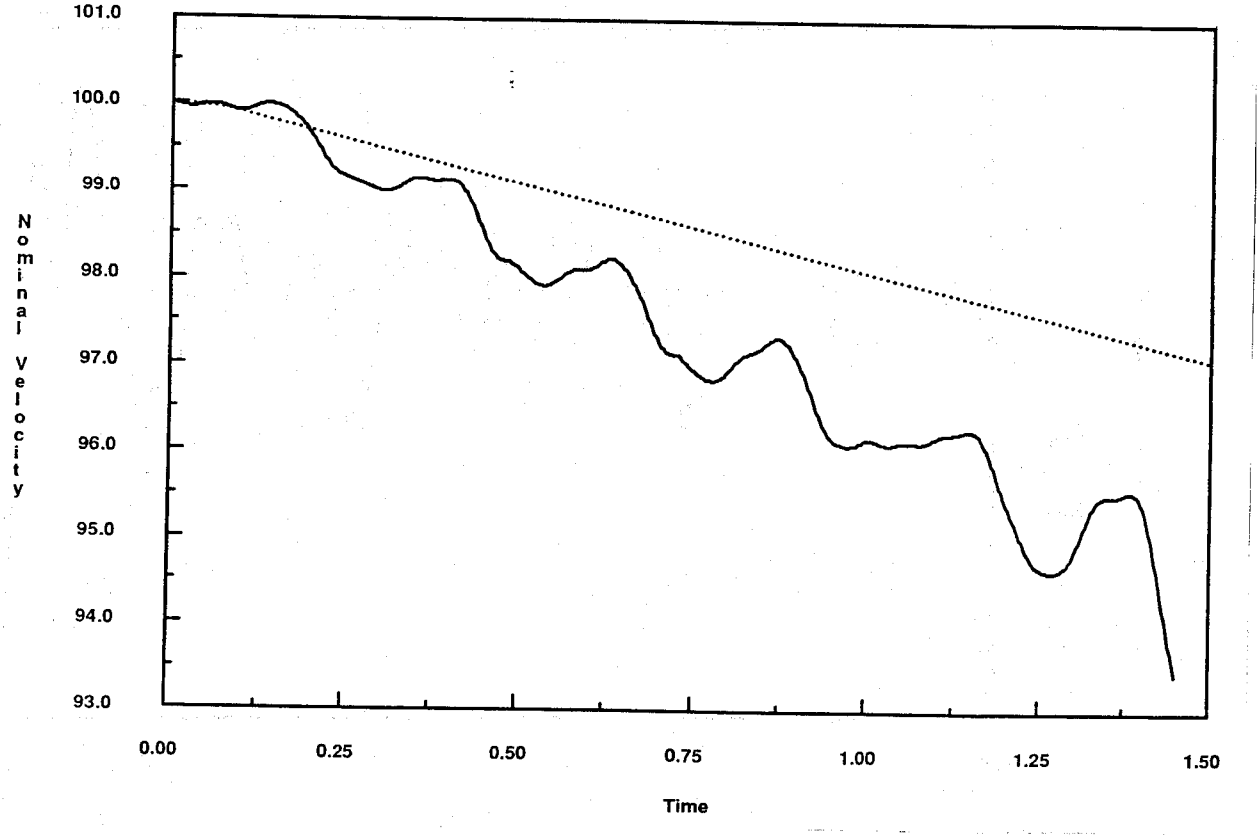

Figure 6.4b. *Effects of braking on vehicle/structure system.* Nominal velocity vs. Time. Six-span beam. Initial velocity $\dot{Y}^1(0) = 100m/s$. Solid line: flexible structure and unknown nominal motion. Dotted line: rigid structure, or flexible structure with prescribed nominal motion.

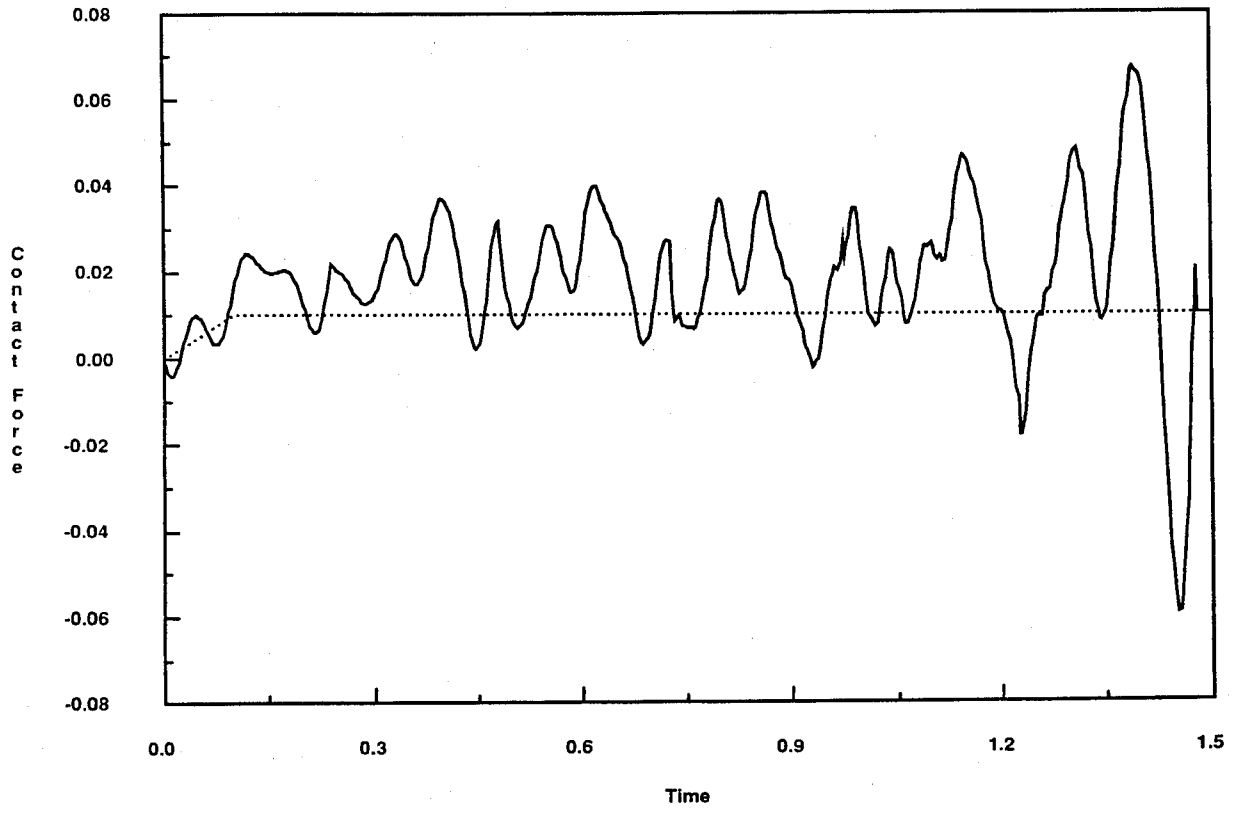

Figure 6.4c. *Effects of braking on vehicle/structure system.* Horizontal contact force F_c^1 (normalized wrt vertical force $|F^2|$) vs. Time. Solid line: flexible structure and unknown nominal motion. Dotted line: rigid structure. $\dot{Y}^1(0) = 100m/s$.

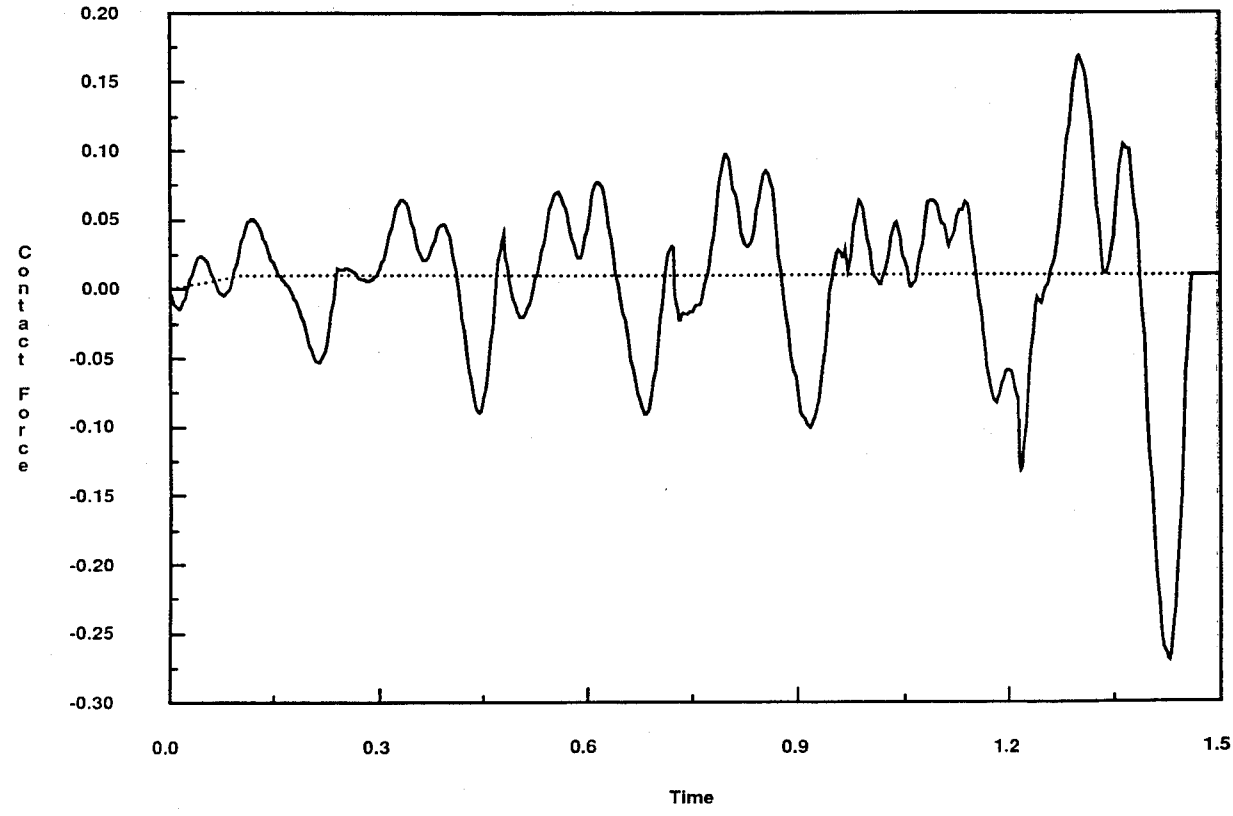

Figure 6.4d. *Effects of braking on vehicle/structure system.* Horizontal contact force F_c^1 (normalized wrt vertical force $|F^2|$) vs. Time. Solid line: flexible structure and prescribed nominal motion. Dotted line: rigid structure. $\dot{Y}^1(0) = 100m/s$.